Final Report for AOARD Grant FA2386-10-1-4044	
Title	Exploratory Research and Development of Microwave Filters in Silicon Technology
Date	September 25 2013
Name of PI	Dr. Koen Mouthaan
E-mail address	k.mouthaan@nus.edu.sg
Institution	National University of Singapore
Mailing Address	4 Engineering Drive 3
Phone	(+65)-6516-7871
Fax	(+65)-6779-1103
Period of Performance Month/Day/Year-Month/Day/Year	07/01/2010 – 06/30/2012

This material is based on research sponsored by the Air Force Research Laboratory, under agreement number FA2386-10-1-4044. The U.S. Government is authorized to reproduce and distribute reprints for governmental purposes notwithstanding any copyright notation thereon. The views and conclusions contained herein are those of the authors and should not be interpreted as necessarily representing the official policies or endorsements, either expressed or implied, of the Air Force Research Laboratory or the U.S. Government.

Report Documentation Page

Form Approved
OMB No. 0704-0188

1. REPORT DATE	2. REPORT TYPE	3. DATES COVERED
26 SEP 2013	**Final**	**01-07-2010 to 30-12-2012**

4. TITLE AND SUBTITLE
Exploratory Research and Development of Microwave Filters in Silicon Technology

5a. CONTRACT NUMBER
FA23861014044

5b. GRANT NUMBER

5c. PROGRAM ELEMENT NUMBER

6. AUTHOR(S)
Koenraad Mouthaan

5d. PROJECT NUMBER

5e. TASK NUMBER

5f. WORK UNIT NUMBER

7. PERFORMING ORGANIZATION NAME(S) AND ADDRESS(ES)
National University of Singapore,4 Engineering Drive 3,Singapore 117576,Singapore,SP,117576

8. PERFORMING ORGANIZATION REPORT NUMBER
N/A

9. SPONSORING/MONITORING AGENCY NAME(S) AND ADDRESS(ES)
AOARD, UNIT 45002, APO, AP, 96338-5002

10. SPONSOR/MONITOR'S ACRONYM(S)
AOARD

11. SPONSOR/MONITOR'S REPORT NUMBER(S)
AOARD-104044

12. DISTRIBUTION/AVAILABILITY STATEMENT
Approved for public release; distribution unlimited

13. SUPPLEMENTARY NOTES

14. ABSTRACT
The objective of the project is the design of an L-band filter and a Ka filter in a standard 0.13 um CMOS process. Four different microwave filters have been designed and tested in a standard 0.13 μm CMOS process. For the first filter a new effective method to suppress the common-mode in a purely passive CMOS L-band filter is presented. For the second filter a 7-stage L-band bandpass filter using active series and shunt inductors is demonstrated in a standard 0.13 μm CMOS process. For the third filter a Ka band filter in 0.13 μm CMOS is presented. The filter with improved selectivity consists of BCCPS, CPS sections and MIM capacitors. For the fourth filter a CMOS Ka-band lumped element DBR filter is presented utilizing CMOS spiral inductors and MIM capacitors.

15. SUBJECT TERMS
microwave filters

16. SECURITY CLASSIFICATION OF:			17. LIMITATION OF ABSTRACT	18. NUMBER OF PAGES	19a. NAME OF RESPONSIBLE PERSON
a. REPORT	b. ABSTRACT	c. THIS PAGE			
unclassified	**unclassified**	**unclassified**	**Same as Report (SAR)**	**55**	

Abstract

The objective of the project is the design of an L-band filter and a K_a filter in a standard 0.13 um CMOS process.

Four different microwave filters have been designed and tested in a standard 0.13 μm CMOS process.

For the first filter a new effective method to suppress the common-mode in a purely passive CMOS L-band filter is presented. In the differential-mode the filter's bandwidth is from 1 GHz to 1.9 GHz (62%), the insertion loss is 3.15 dB, and the return loss is better than 12.3 dB in the passband. The common-mode is suppressed for 23.5 dB even up to 3.7 GHz. Furthermore, a very small sample to sample performance variation was found in measurement.

For the second filter a 7-stage L-band bandpass filter using active series and shunt inductors is demonstrated in a standard 0.13 μm CMOS process. The measured 3 dB bandwidth is from 1-2 GHz and the passband ripple is within 0.5 dB. The measured out-of-band rejection is better than 40 dB below 0.7 GHz and above 2.24 GHz. The input return loss is better than 8 dB. The measured common mode suppression is higher than 30 dB and the input referred 1 dB compression point is -21 dBm. The whole filter draws a current of 25 mA from a 1.2 V voltage supply.

For the third filter a K_a band filter in 0.13 μm CMOS is presented. The filter with improved selectivity consists of BCCPS, CPS sections and MIM capacitors. BCCPS facilitates the realization of a compact resonator with a high coupling coefficient. Furthermore, this resonator introduces a transmission zero at DC. The filter selectivity is furthered improved by adding a zero below and a zero above the passband using stubs and capacitors. The realized filter has small size compared to the wavelength which makes it suitable even for lower frequency IC design. The insertion loss can be reduced by using a lower loss process, improved modeling of components and application of loss compensation techniques.

For the fourth filter a CMOS K_a-band lumped element DBR filter is presented utilizing CMOS spiral inductors and MIM capacitors. The proposed lumped element DBR filter is easy to be implemented which reduces simulation time and design complexity. Moreover, this topology can be used in lower microwave frequency design without increasing the filter size and with improved insertion loss. The measured filter realizes high notch rejections. This demonstrates that CMOS passive elements are useful components when designing a filter with transmission zeros for a sharper cut-off response.

Table of Contents

1. Introduction 6

2. L-band wideband filter with high common-mode rejection 10

2.1. Introduction 10

2.2. Filter Topology 11

2.3. Filter Design 13

A. Common-Mode Suppression Method I 14

B. Common-Mode Suppression Method II 16

2.4. Filter Results and Discussion 16

2.5. Conclusion 19

3. Active inductor based L-band bandpass filter with High out-of-band rejection 20

3.1. Introduction 20

3.2. Active Inductor based Resonator 21

A. Gyrator Based Active Inductor 21

B. Transconductor Design 23

C. Active Inductor Based Resonator 23

3.3. Bandpass Filter Implementation 24

3.4. Measurement Results 25

3.5. Conclusion 29

4. Compact K_a band filter in 0.13 μm CMOS using broadside coupled coplanar stripline 30

4.1. Introduction 30

4.2. Analysis and Design 32

A. BCCPS 32

B. Analysis of BCCPS in CMOS 35

4.3. CMOS K_a band filter using BCCPS section 38

4.4. Filter details 39

4.5. Filter results 40

4.6. Conclusions 43

5. A K_a-Band Lumped Element Dual-Behavior Resonator (DBR) Filter in Standard 0.13-μm CMOS Technology 44

5.1. Introduction 44

5.2. Lumped Element DBR Filter Design 45

5.3. Experimental Results 49

5.4. Conclusions 51

6. Conclusions and Future Work 52

1. INTRODUCTION

The objective of the project is design of an L-band filter and a K_a filter.

The specifications of the two filters are shown below.

Notional Filter Specifications L-Band Filter		
Requirement	**Value**	**Units**
Type	Band pass	
Input Impedance	50	Ohms
Input Type	Differential	
Input Return Loss	15	dB
Output Impedance	50	Ohms
Output Type	Differential	
Output Return Loss	15	dB
Pass Band Frequency	1 - 2	GHz
Pass Band Loss	< 3	dB
Pass Band Ripple	< 2	dB
Out of Band Rejection		
Low side @ 0.75 GHz	>40	dB
High Side @ 2.25 GHz	>40	dB
Note 1: Rejection loss is relative to pass band loss Note 2: Prefers passive filter topology		

Notional Filter Specifications K_a-Band Filter		
Requirement	**Value**	**Units**
Type	Band pass	
Input Impedance	50	Ohms
Input Type	Single Ended	
Input Return Loss	15	dB
Output Impedance	50	Ohms
Output Type	Single Ended	
Output Return Loss	15	dB
Pass Band Frequency	27-28	GHz
Pass Band Loss	< 3	dB
Pass Band Ripple	< 2	dB
Out of Band Rejection		
Low side @ 25.75 GHz	>35	dB
High Side @ 29.25 GHz	>35	dB
Note 1: Rejection loss is relative to pass band loss Note 2: No preference on using passive or active filter topology		

Four different microwave filters have been designed and tested in a standard 0.13 μm CMOS process.

1. A passive L-band wideband filter with high common-mode rejection is discussed in Chapter 2. The work was published in "L-band wideband filter in 0.13 μm CMOS with high common-mode rejection", A. Taslimi, K. Mouthaan, IEEE MTT-S International Microwave Symposium, 2012 [1].
2. An active L-band bandpass filter based on active inductors is discussed in chapter 3. The work was published in "Lossless CMOS active reciprocal two-port inductor and application in a series LC filter", F. Hu, K. Mouthaan, 42nd European Microwave Conference, 2012 [2].
3. A compact K_a-band filter using broadside coupled coplanar stripline is demonstrated in chapter 4. The results will be presented in "Compact Ka Band Filter in 0.13 μm CMOS Using Broadside Coupled Coplanar Stripline", A. Taslimi, K. Mouthaan, 43nd European Microwave Conference, 2012 [3].
4. A K_a-Band Lumped Element Dual-Behavior Resonator (DBR) Filter is demonstrated in chapter 5. The filter will be presented in "A K_a-Band Lumped Element Dual-Behavior Resonator (DBR) Filter in Standard 0.13-μm CMOS Technology", X. Lu, K. Mouthaan, T.-S. Yeo, Asia Pacific Microwave Conference, 2013 [4].

The first L-band CMOS filter with high common-mode rejection covering a wide bandwidth has a high differential out-of-band rejection over a large frequency range. The high common-mode rejection in the passband is realized by shifting the common-mode transmission zeros into the passband while maintaining the differential-mode bandpass response. The measured differential-mode insertion loss and return loss of the filter with 62% bandwidth from 1 GHz to 1.9 GHz are better than 3.2 dB and 12.3 dB, respectively. The common-mode rejection is more than 23.5 dB up to 3.7 GHz.

The second design is an active 7-stage L-band bandpass filter with high out-of-band rejection. The active filter employs active shunt and series inductors. The fabricated active bandpass filter occupies 0.18 mm^2 area and has a 3 dB bandwidth from 1 GHz to 2 GHz. The measured out-of-band rejection is better than 40 dB below 0.7 GHz and above 2.24 GHz. A common mode suppression better than 30 dB is obtained. The measured input referred 1 dB compression point is -21 dBm and the filter consumes 25 mA at 1.2 V supply voltage.

The third design, a K_a-band bandpass filter in 0.13 μm CMOS, has good out-of-band rejection and a good shape factor. These features are facilitated by the use of broadside coupled coplanar stripline (BCCPS). The filter consists of a BCCPS section, coplanar striplines (CPS), and MIM capacitors. We derive the characteristic impedance and effective dielectric

constant of the BCCPS in CMOS and apply it to the design of the bandpass filter. The realized filter has a measured 3 dB bandwidth from 25.5 GHz to 31.6 GHz (21%). The measured insertion loss is 6.9 dB and the size is 0.6 x 0.3 mm^2 excluding pads. The filter rejection below 18 GHz and above 41 GHz is better than 35 dB.

In the fourth design, a Ka-band bandpass filter is designed and measured. The input return loss is better than 14 dB and output return loss is better than 16.5 dB in the passband. The measured filter also achieves a 3-dB bandwidth of 15% and realizes two transmission zeros at 20.2 GHz and 37 GHz. Compared to the reported CMOS DBR filters based on SIRs and open stubs, this filter achieves higher rejections of 48 dB by using lumped elements resonators. This demonstrates that lumped element resonators are useful to create transmission zeros in CMOS chip filter design.
The four filter designs are reported in the following chapters.

2. L-BAND WIDEBAND FILTER WITH HIGH COMMON-MODE REJECTION

2.1. Introduction

The demand for wideband balanced circuits realized in low-cost integrated circuits, including filters, is increasing for application in broadband communication and radar systems. Compared to single-ended circuits, balanced circuits have higher noise immunity while they can suppress the common-mode (CM) [5]. Moreover, in a balanced system, it is desirable to design all the circuits fully balanced to avoid conversions from single-ended to balanced circuits.

For integrated circuits, several active balanced filters have been reported [6]. Active filters can compensate for losses but they suffer from poor linearity, low stability and increased noise level. In addition, they consume power. Passive filters offer a larger dynamic range without the need for a power supply. However, they suffer from loss, especially when integrated in CMOS technology. Wideband balanced passive filters on PCB with 110%, 123% and 62% bandwidth and 20, 25 and 20 dB CM rejection are presented in [5], [7, and [8] respectively. However, these filters are based on transmission lines. The CM rejection is essential for balanced filters to increase the signal-to-noise ratio [8].

We present a passive balanced L-band filter in CMOS process. For realization of the filter in CMOS the use of transmission line circuits is not feasible due to their long lengths. Therefore, only a lumped element circuit design is feasible at these frequencies. For a balanced L-band filter,

a passband from 1-2 GHz in differential-mode (DM) is required together with an effective suppression of the CM. However, the typical CM rejection of a balanced wide-band filter is very poor (Fig. 1). Here we present a new method to achieve the wideband balanced L-band filter in CMOS while achieving a high passband CM rejection.

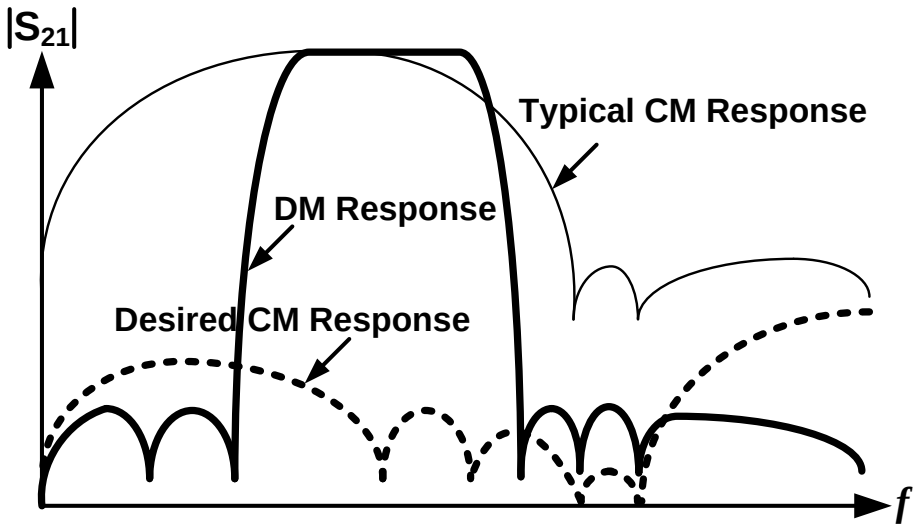

Fig. 1. Typical differential-mode (DM) and common-mode (CM) responses and desired suppressed CM by zero shifting.

2.2. Filter Topology

The proposed filter circuit is shown in Fig. 2(a). Each series and shunt resonator is a combination of a parallel LC tank in series with a capacitor as shown in Fig. 2(b). Each resonator has two critical frequencies: open circuit frequency f_{oc} and short circuit frequencyf_{sc}. Since f_{sc}<f_{oc}, the pole of the series resonator is below its zero, while for shunt resonators it is the opposite. The proposed filter has also inherent transmission zeros at zero and infinity. This filter has less inductors compared to Chebyshev

and elliptic filters. Furthermore, it is easier to design a single ended filter in the first step as illustrated in Fig. 3. The proposed method for placing the zeros and poles for a filter with passband from f_1 to f_2 is as follows:

- Select the starting points of the low and high frequency rejection bands $f_{l,1}$, $f_{h,1}$ as two first transmission zeros.
- Second low frequency rejection zero is: $f_{l,2} = f_{l,1}^2/f_1$.
- Second high frequency rejection zero is: $f_{h,2} = f_{h,1}^2/f_2$.
- Other zeros: $f_{h,i+1=} f_{h,i}^2/f_{h,i-1}$, $f_{l,i+1=} f_{l,i}^2/f_{l,i-1}$ (i>2).
- All poles are at the center frequency f_o i.e. $\sqrt{f_1.f_2}$.

There is one degree of freedom for each resonator (three unknown variables i.e. L, C, C´ and two determined values i.e. f_{oc}, f_{sc}). Since, there are limitations for inductor values and Q factor, this degree of freedom is assigned to the resonator's inductor. After selecting inductor values, the capacitor values are calculated based on the locations of the zero and the pole. The abovementioned placement of zeros and poles is only one possible solution and requires optimization. After optimizing the inductor and capacitor values, the balanced filter is determined by mirroring the single-ended version (Fig. 2(a)). Note that the ground of the single-ended version in the shunt branches should be removed as shown in Fig. 4(a). The abovementioned method is also applicable for higher order filters.

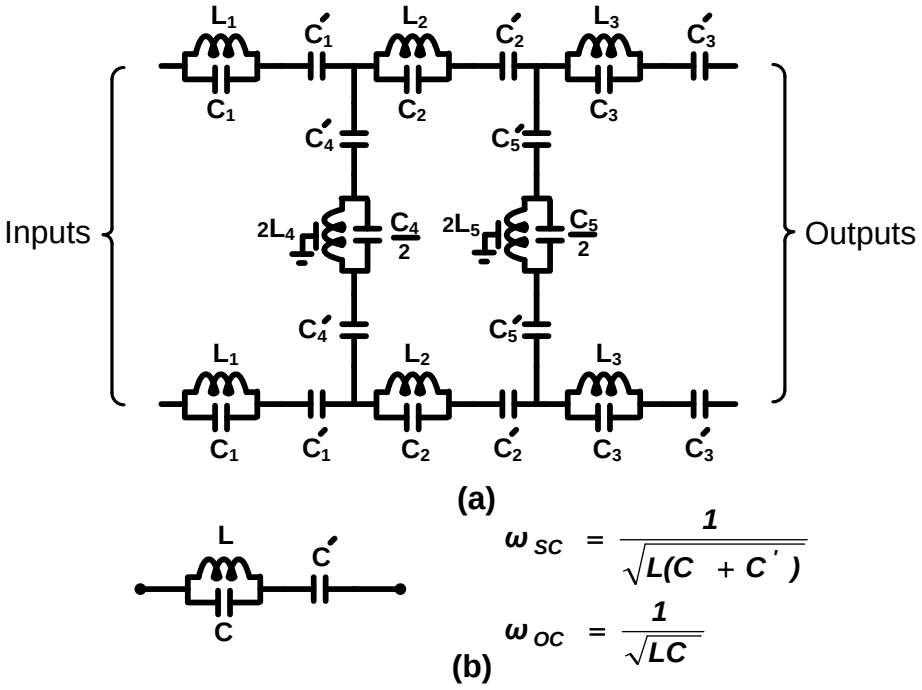

Fig. 2. (a). Proposed LC balanced filter. (b) Series and shunt resonator structures.

2.3. Filter Design

A wideband bandpass filter from 1 GHz to 2 GHz using the proposed topology in Fig. 2(a) has been designed in a standard 0.13 μm CMOS. Our filter requirements include:

- DM insertion loss less than 3 dB
- DM rejection larger than 40 dB below 0.75 GHz
- DM rejection larger than 40 dB above 2.25 GHz
- CM rejection larger than 25 dB from 1-2 GHz

Based on the method outlined in the previous section, DM transmission zeros are placed at:

- $f_{l,1}$=0.75 GHz, $f_{h,1}$=2.25 GHz (two rejection bands starting points).
- $f_{l,2}$= 0.56 GHz, $f_{h,2}$=2.53 GHz, $f_{h,3}$=2.84 GHz.

- f_o=1.4 GHz.

Note, the filter inherently has also two transmission zeros at zero and at infinity. To suppress the CM, it is necessary to modify the shunt resonators. In the following we present and compare two methods.

A. Common-Mode Suppression Method I

In the first method we ground one of the tank components while keeping the other tank component ungrounded. As shown in Fig.4(b), the shunt resonator behaves differently for CM and DM excitations. The selected component could be the capacitor or the inductor of the tank. Grounding the tank's capacitor introduces a CM zero at infinity. However, grounding the tank's inductor introduces a new finite CM transmission zero. Therefore we selected the inductor to be grounded which provides another finite CM transmission zero. For narrowband applications the tank's shunt capacitor's C is much larger than the series capacitor C´. Consequently, in the CM, when C is eliminated there is a large frequency shift in the transmission zero. However, for moderate bandwidths, C and C´ are in the same range. As a result, eliminating C will not change the location of the transmission zero very much.

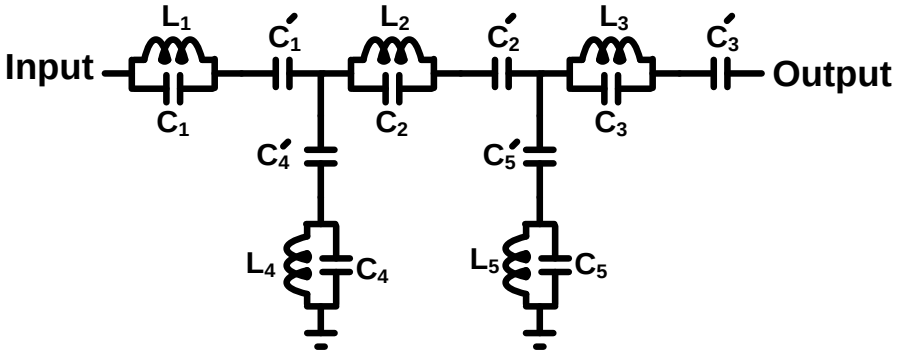

Fig. 3. Single-ended topology (DM equivalent circuit).

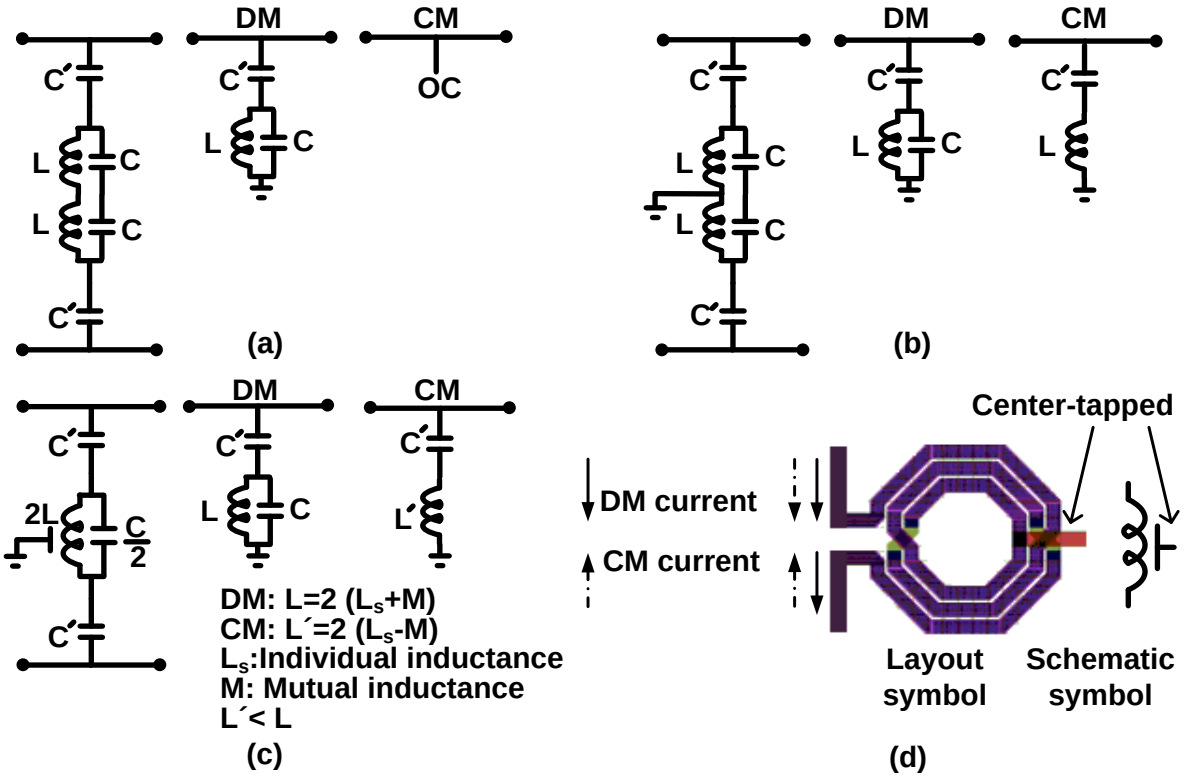

Fig. 4. (a) Ungrounded shunt branch and equivalent DM and CM (b) Shunt branch and equivalent DM and CM for Method I. (c) Shunt branch and equivalent DM and CM for Method II. (d) DM and CM current directions in a shunt center-tapped inductor.

B. Common-Mode Suppression Method II

In the second method instead of applying two identical inductors in the shunt branches and grounding their common node, as illustrated in Fig. 4(b), a center-tapped grounded inductor can be replaced as shown in Fig. 4(c). This method reduces the size, improves the quality factor, and also suppresses the CM effectively. As shown in Fig. 4(d), in the DM the magnetic coupling between the inductors increases the total inductance, because the current has the same direction in both inductors. However, in the CM, these currents are in the opposite direction which reduces the overall inductance [9]. Consequently, in the CM the location of the transmission zero shifts to higher frequencies and even into the passband and suppresses the CM within the passband.

2.4. Filter Results and Discussion

Fig. 5 shows the simulated S-parameters results of the filter for the three cases discussed earlier: no CM suppression, CM suppression using method I, and using method II. The comparison shows that using grounded center-tapped inductors very effectively suppresses the CM insertion loss $|S_{21}^{cc}|$ without affecting the DM insertion loss $|S_{21}^{dd}|$ and return loss $|S_{11}^{dd}|$. Therefore we used method II in the fabricated filter, which is shown inFig. 6. The simulated results and measured results for six samples are shown in Fig. 7(a). Good agreement between simulation and measurement is observed. Also, very little spread between the six samples is found. The filter is measured using a four-port vector network analyzer and the S-

parameters for the DM and CM are extracted using the procedure outlined in [10]. The measured filter has a 3 dB DM bandwidth of 62% from 1 GHz to 1.9 GHz and a 40 dB DM rejection below 0.75 GHz and above 2.25 GHz up to 10 GHz. The return loss is better than 12.3 dB in the passband and the insertion loss is 3.15 dB. The CM is suppressed by more than 23.5 dB up to 3.7 GHz. CM suppression is maintained around 3 GHz due to the zeros in the series branches and by our placement of the CM transmission zeros of the shunt branches. Since there is no CM transmission zero at infinity, the CM rejection above 3 GHz is less than the DM rejection. A wider view of measured results up to 40 GHz is illustrated in Fig. 7(b). A high differential out-of-band rejection over a large frequency range is achieved.

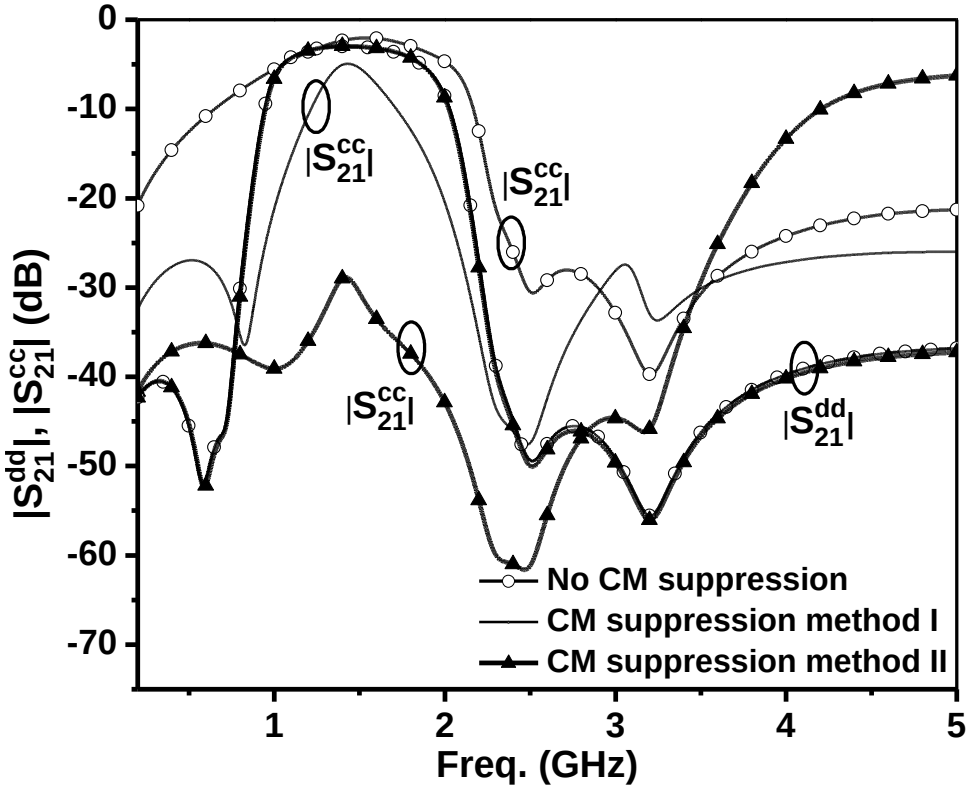

Fig. 5. Simulated DM and CM results for three cases in Fig. 4.

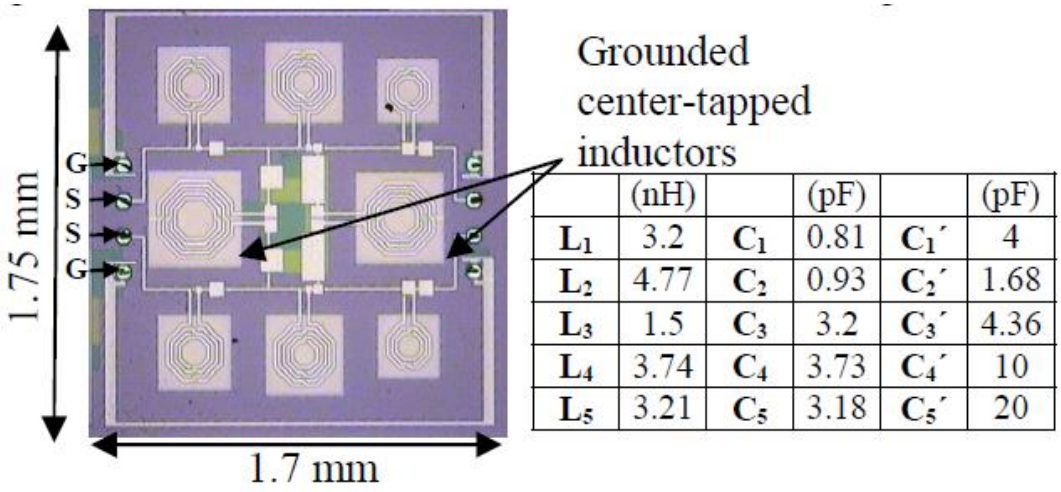

	(nH)		(pF)		(pF)
L_1	3.2	C_1	0.81	C_1'	4
L_2	4.77	C_2	0.93	C_2'	1.68
L_3	1.5	C_3	3.2	C_3'	4.36
L_4	3.74	C_4	3.73	C_4'	10
L_5	3.21	C_5	3.18	C_5'	20

Fig. 6. Die photograph and components values at 1.5 GHz.

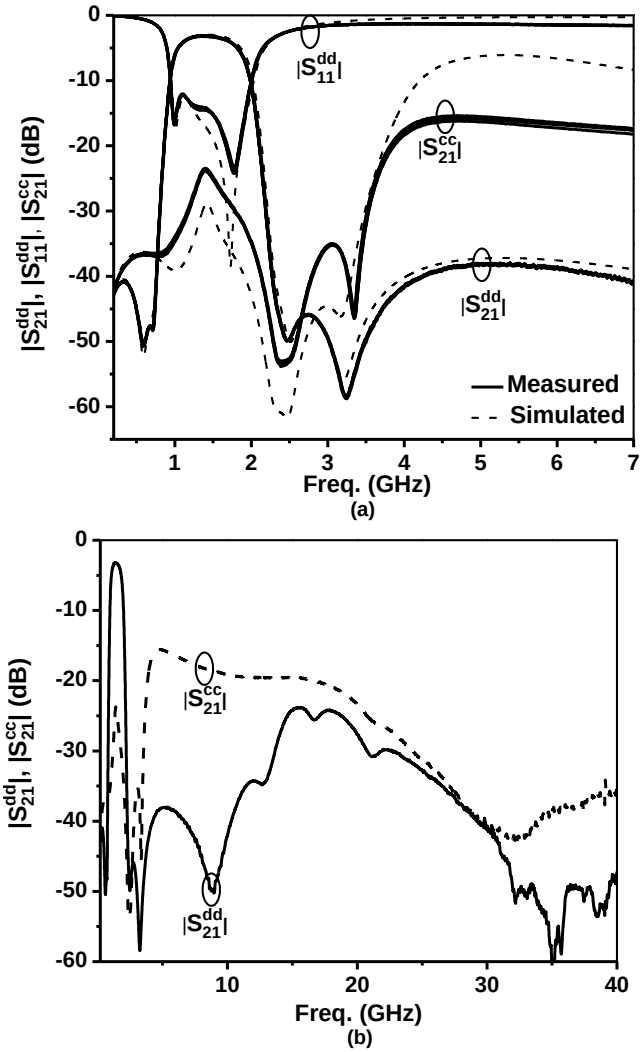

Fig. 7. (a) Simulated and measured results. (b) Measured results for a wider frequency range.

2.5. Conclusion

A new effective method to suppress the common-mode in a purely passive CMOS L-band filter is presented. In the differential-mode the filter's bandwidth is from 1 GHz to 1.9 GHz (62%), the insertion loss is 3.15 dB, and the return loss is better than 12.3 dB in the passband. The common-mode is suppressed for 23.5 dB even up to 3.7 GHz. Furthermore, a very small sample to sample performance variation was found in measurement.

3. ACTIVE INDUCTOR BASED L-BAND BANDPASS FILTER WITH HIGH OUT-OF-BAND REJECTION

3.1. Introduction

To realize low cost system-on-a-chip (SOC), great efforts have been made to integrate RF components for wireless applications onto a single CMOS chip. RF filters, a key frequency selective component, have also been successfully realized in CMOS technology, e.g. [11]-[16]. However, the realization of CMOS on-chip bandpass filters with flat passband and high out-of-band rejection still faces problems due to the loss of passive resonators.

One solution is to introduce negative resistance in the passive components to compensate losses [11]-[14]. Transmission line based resonators compensated by negative resistors are utilized in filter design [11]. A drawback is that higher order filters with better frequency selectivity require a large area. Active compensations directly applied to the major lossy components of inductors are introduced in [12] and [13]. However, achieving good frequency selectivity within a small chip area remains an issue.

Another approach to realize filters with good frequency selectivity is to use active inductors [14]-[20]. However, the filters generally have a low order response and are more suitable for narrow band applications, because the active inductors employed are one port shunt inductors to ground.

To develop higher order bandpass filters with a flat passband response and decent frequency selectivity, high Q differential active reciprocal two-port inductors in series configuration, based on [17], are employed here. Together with conventional active shunt inductors, an L-band bandpass filter is then designed.

3.2. Active Inductor based Resonator

A. Gyrator Based Active Inductor

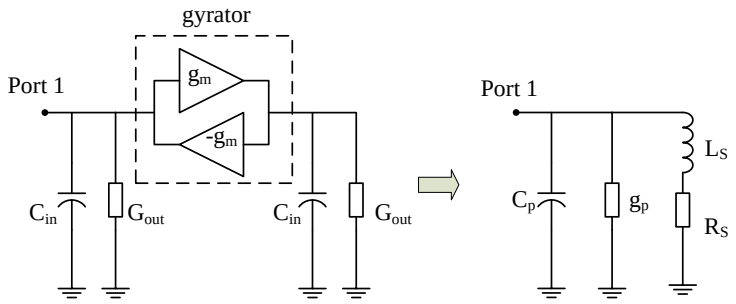

Fig. 8. Gyrator based active shunt inductor.

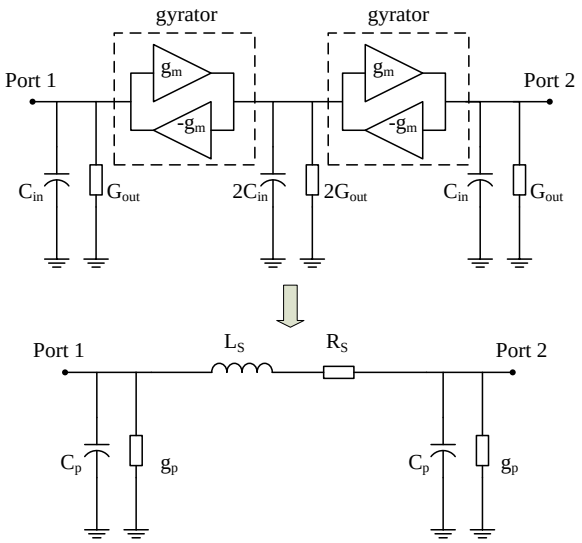

Fig. 9. Gyrator based active series inductor.

Fig. 8 shows the gyrator based active inductor circuit and the equivalent lumped model [17]. The shunt realization and the series two-port realization are shown in Fig. 8 and Fig. 9 respectively. The active shunt inductor has already been widely investigated [22]-[28]. Therefore, this part focuses on the active series inductor as the results can be easily extended to the active shunt inductor.

As shown in Fig. 9, an active series inductor is realized by cascading two gyrator cells. The typical parasitic components of a transconductor with a transconductance of g_m are simplified to an input capacitance C_{in} and an output admittance G_{out}. The equivalent model for the active inductor with parasitic components is also shown in Fig. 9. The values of the equivalent model are given by [17]:

$$R_S = 2G_{out} / g_m^2 \tag{11}$$

$$L_S = 2C_{in} / g_m^2 \tag{12}$$

$$C_p = C_{in} \tag{13}$$

$$G_p = G_{out} \tag{14}$$

The quality factor of the realized inductor is related to the series resistance R_S as well as the parallel conductance G_p. Thus, the quality factor of the active inductor can be improved by minimizing the output admittance G_{out}.

B. Transconductor Design

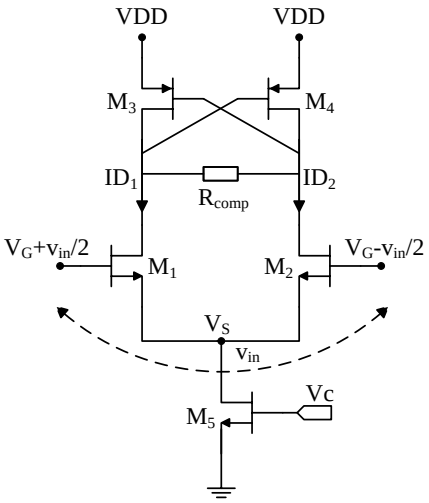

Fig. 10. Differential Transconductor

The circuit of the differential transconductor is shown in Fig. 10. The major advantage of the differential arrangement is that the input-output characteristics of the transconductor will not change while generating positive and negative transconductances. The transconductor design is aimed to achieve a wide bandwidth of the overall transconductance (Gm). This work directly employs the cross coupled cell as an active load to reduce the output parasitics as well as the power consumption.

C. Active Inductor Based Resonator

An LC resonator can be realized with the active inductor. However, the parasitic capacitance to ground may affect the performance. A series LC resonator composed of ideal inductors is compared with its active realization in Fig. 11. The resonator is used to generate a transmission zero.

Discrepancies are observed and the return loss is worse due to the parasitic capacitances to ground introduced by the active series inductor. Therefore these extra capacitances should be embedded in the filter design.

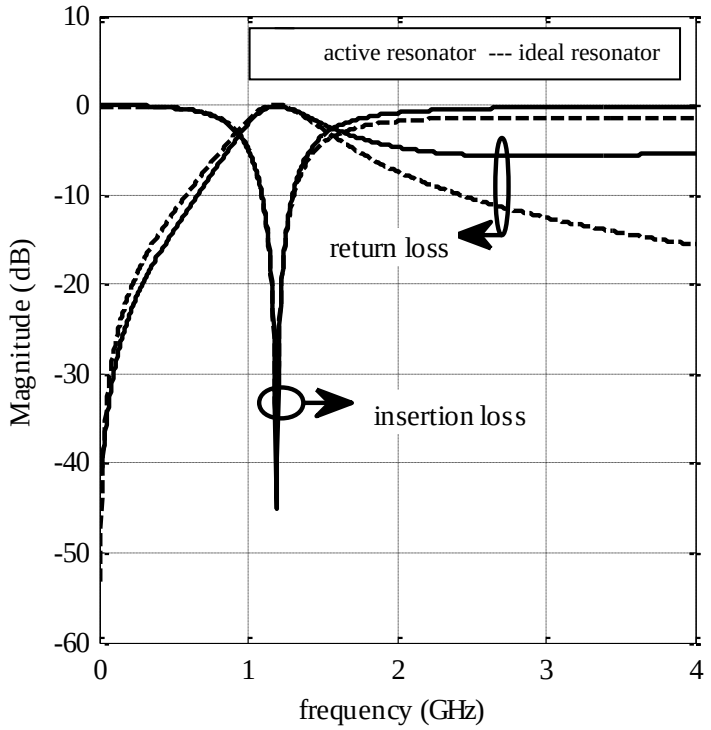

Fig. 11. Active inductor based resonator versus ideal LC resonator

3.3. Bandpass Filter Implementation

For active wideband bandpass filter design, the parasitic capacitors of the active inductors are inevitable and will deteriorate the performance to a large extent. As shown in Fig. 8 and Fig. 9, these parasitic capacitors are mainly introduced by the input and output capacitors of the transconductor cells. To address this problem, the parasitic capacitors are embedded in the filter design.

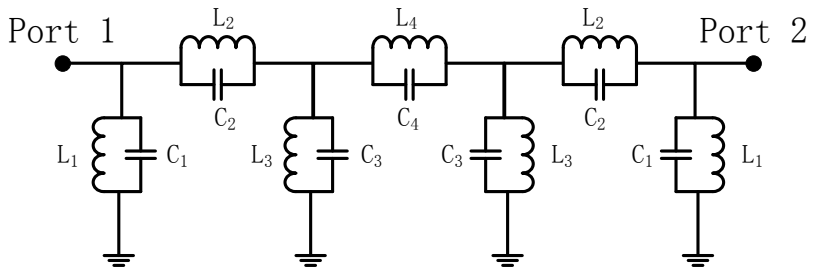

Fig. 12. Proposed 7-stage bandpass filter prototype.

The schematic of a 7-stage wideband bandpass filter is shown in Fig. 12. The first merit of this prototype is that the shunt capacitors C_1 and C_3 are capable of absorbing the parasitic shunt capacitors of the active realizations of the inductors L_1 to L_4. Moreover, this prototype can provide three transmission zeros, which further improves the frequency selectivity of the bandpass filter. The pass band is set to cover the whole L-band, from 1 GHz to 2 GHz, resulting in an octave bandwidth. In this design, resonators are symmetrically arranged. Two identical transmission zeros, generated by the two parallel resonators with L_2 and C_2, are located at 2.25 GHz and the other transmission zero, provided by the resonator with L_4 and C_4, is set at 3.5 GHz. Please note that the proposed techniques are also suitable for the design of filters with other bandwidths and center frequencies.

3.4. Measurement Results

The L-band 7-stage bandpass filter with active inductors is fabricated in a standard 0.13 μm CMOS process. The micrograph of the fabricated bandpass filter is shown in Fig. 13. The core part including transistors and

filter capacitors is 1x0.18 mm^2. The differential active bandpass filter is measured as a four-port device with wafer probes. DC biasing is applied from a PCB using bonding wires. A four-port calibration is performed before the measurement. The 7-stage differential bandpass filter draws a current of 25 mA at a 1.2 V supply voltage.

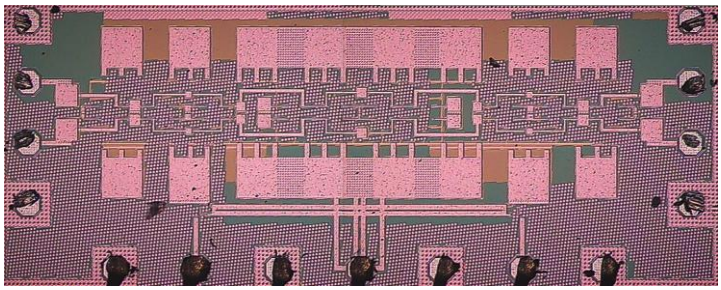

Fig. 13. Micrograph of the fabricated 7-stage bandpass filter.

The measured differential mode transmission coefficients and reflection coefficients are shown in Fig. 14. The forward and backward transmission differs due to the mismatch in the layout. The measured out-of-band rejection is better than 40 dB below 0.7 GHz and above 2.24 GHz. Unlike many microstrip-line based bandpass filters, there is no parasitic passband in the high frequency range. The input return loss is better than 10 dB from 1.1 GHz to 1.98 GHz. At the edges of the passband, the worst input return loss is 8 dB, which may be due to the fabrication variations because the compensating resistor R_{comp} plays a significant role in input and output matching.

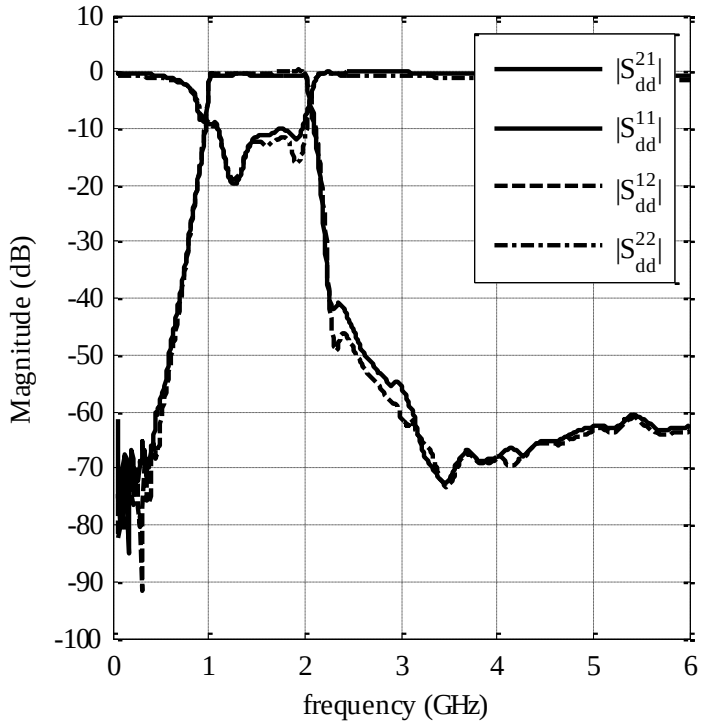

Fig. 14. Measured differential mode S-parameters.

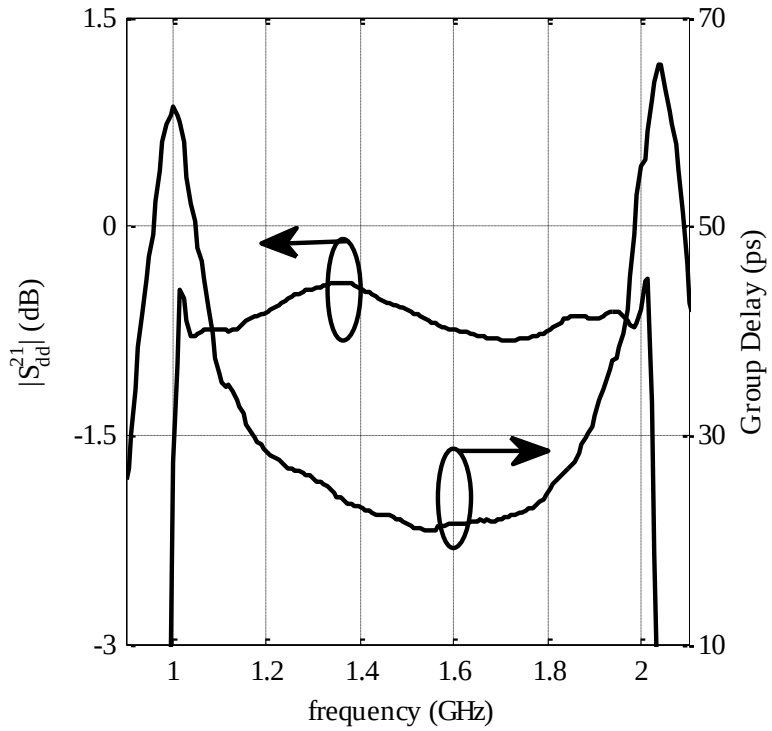

Fig. 15. Enlarged passband response.

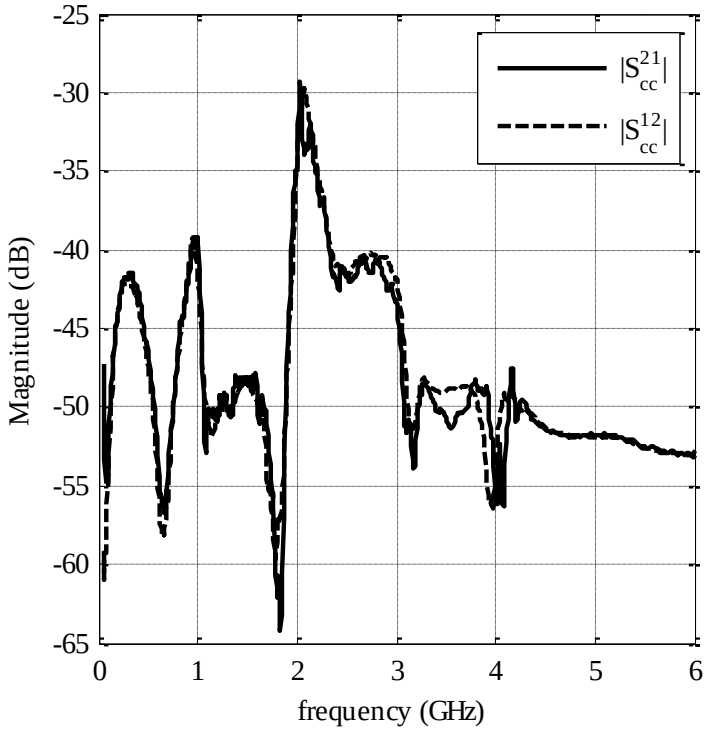

Fig. 16. Measured common mode transmission coefficients.

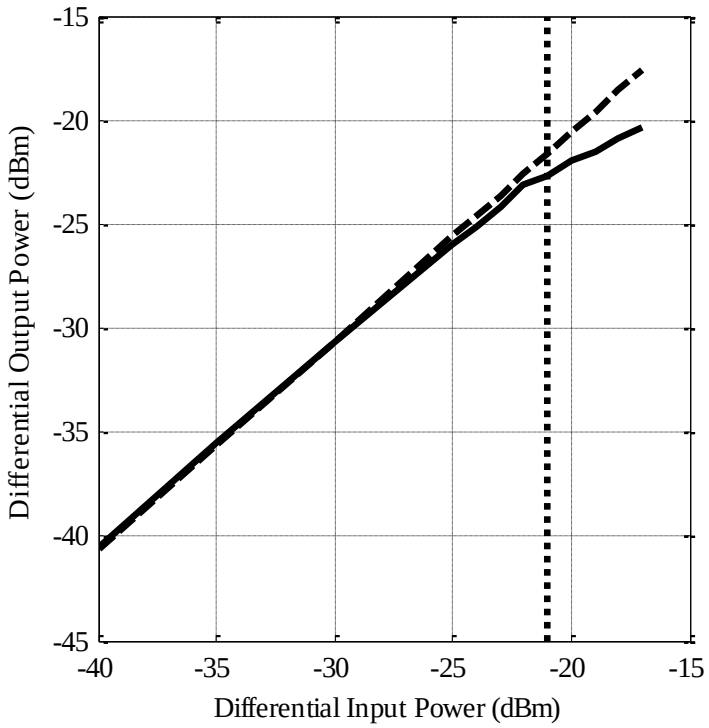

Fig. 17. Measured input 1 dB compression point.

The passband forward transmission is enlarged and shown in Fig. 15. The insertion loss variation in the passband is less than 0.5 dB. The ripples in the passband can be partially attributed to the variations of the compensating resistors. Also shown in Fig. 15 is the group delay of the differential bandpass filter.

The common mode transmission coefficient of the filter is shown in Fig. 16. The suppression is better than 30 dB over the full measured frequency range.

The nonlinear performance is measured with a power source and a spectrum analyzer. A pair of wideband off-chip baluns are used to convert the four-port differential bandpass filter into a two-port single ended device. The input power is swept from -40 dBm to -17 dBm. As shown in Fig. 17, the measured input referred 1 dB compression point is -21 dBm.

3.5. Conclusion

A 7-stage L-band bandpass filter using active series and shunt inductors is demonstrated in a standard 0.13 μm CMOS process. The measured 3 dB bandwidth is from 1-2 GHz and the passband ripple is within 0.5 dB. The measured out-of-band rejection is better than 40 dB below 0.7 GHz and above 2.24 GHz. The input return loss is better than 8 dB. The measured common mode suppression is higher than 30 dB and the input referred 1 dB compression point is -21 dBm. The whole filter draws a current of 25 mA from a 1.2 V voltage supply.

4. COMPACT K_A BAND FILTER IN 0.13 MM CMOS USING BROADSIDE COUPLED COPLANAR STRIPLINE

4.1. Introduction

Complementary metal oxide semiconductor (CMOS) is a widespread integrated circuit technology. Transmission-line based and semi-lumped microwave filters are essential components at high frequency transceivers integrated in this technology. Most of the recently published works on high frequency CMOS filters focus on 60 GHz. The small wavelength at these frequencies makes compact filters feasible for IC integration [28], [29]. There are not too many publications on high performance and compact filters at K band (18-27 GHz) and K_a band (26.5-40 GHz) in CMOS. Low spurious level, low insertion loss and compactness are key requirements for most of the filters. Another key requirement is the shape factor (SF), defined here as the ratio of the 3 dB bandwidth and the 10 dB bandwidth. A SF of 0.6 is considered as the minimum requirement to achieve a reasonable selective response.

A semi-lumped small size filter with a 3 dB fractional bandwidth (FBW) of 17% at 20 GHz and a SF of 0.48 is reported in [30]. The filter size is only $0.91 \times 10^{-3} \lambda_o^2$ due to the lumped components (λ_o is the free space wavelength at the center frequency f_o). Two more K band transmission-line based filters are reported in [31] and [32]. The insertion loss of the microstrip broadside filter in [31] is in the same range as the filter in [10] (i.e. >5 dB) while the FBW of [31] is almost twice of [30]. The filter in [31] has a SF of 0.64 with a comparatively large size of $2.85 \times 10^{-3} \lambda_o^2$. The

semi-lumped filter reported in [32] has low insertion loss considering the bandwidth and a SF of 0.48. However, a spurious response below the passband is observed. A wideband CPW K_a band CMOS filter with 2 dB insertion loss and 78% FBW at 30 GHz is reported in [33]. The filter area is $3.97x10^{-3}\lambda_o^2$.

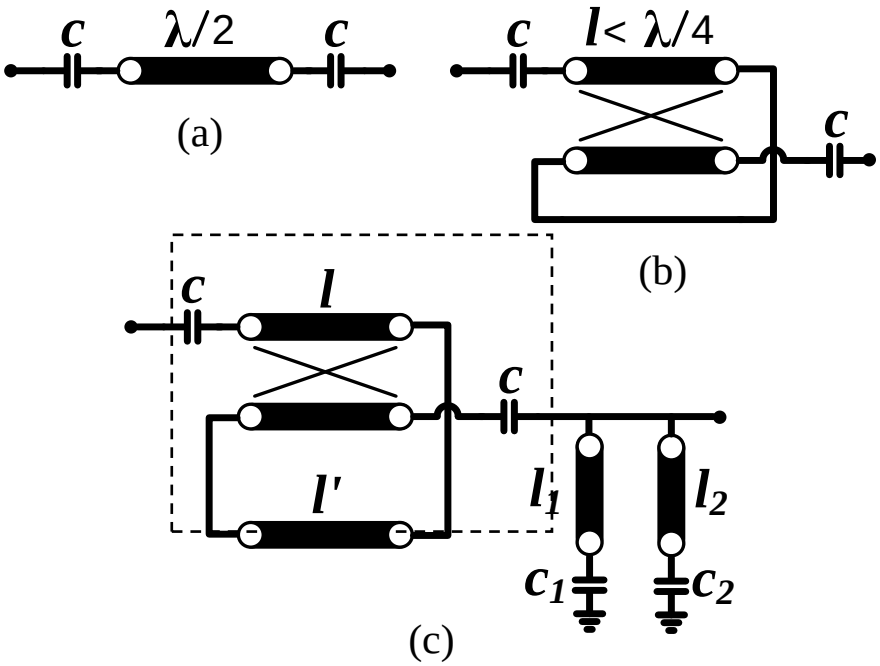

Fig. 18. (a) Half wavelength capacitively loaded resonator. (b) Coupled line capacitively loaded resonator. (c) Proposed filter using coupled line capacitively loaded resonator.

In [34], a K_a band CPW combline filter at 35 GHz is reported with a 16 dB out-of-band rejection below $f_o/2$.

Here, a CMOS K_a band filter at 28.3 GHz with 21% FBW is designed and fabricated in 0.13 μm CMOS. This filter utilizes broadside coupled coplanar stripline (BCCPS). The filter has two additional transmission zeros below and above the passband. The compact filter has a high measured out-of-

band rejection and a good shape factor of 0.63. The minimum insertion loss is 6.9 dB and the size is $1.6x10^{-3}\lambda_o^2$.

4.2. Analysis and Design

A. BCCPS

Transmission-line based filters often suffer from harmonic repetition which may decrease the selectivity of these filters. The half wavelength capacitively loaded resonator, shown in Fig. 8(a), is a high Q resonator when the capacitor is small enough to satisfy the resonant condition [35]. However, the resonator length is relatively large. If the half wavelength transmission line is replace by a coupled line, as shown in Fig. 18(b), the resonator's length can be reduced significantly. To achieve a positive coupling coefficient for a coupled line, the even-mode impedance is always larger than the odd-mode impedance. However, the even-mode dielectric constant can be larger or smaller than the odd-mode dielectric constant. Fig. 19 shows the simulated comparison for three cases. Case I is the half wavelength resonator shown in Fig. 18(a) with characteristic impedance of Z_0 and dielectric constant of ε_r.

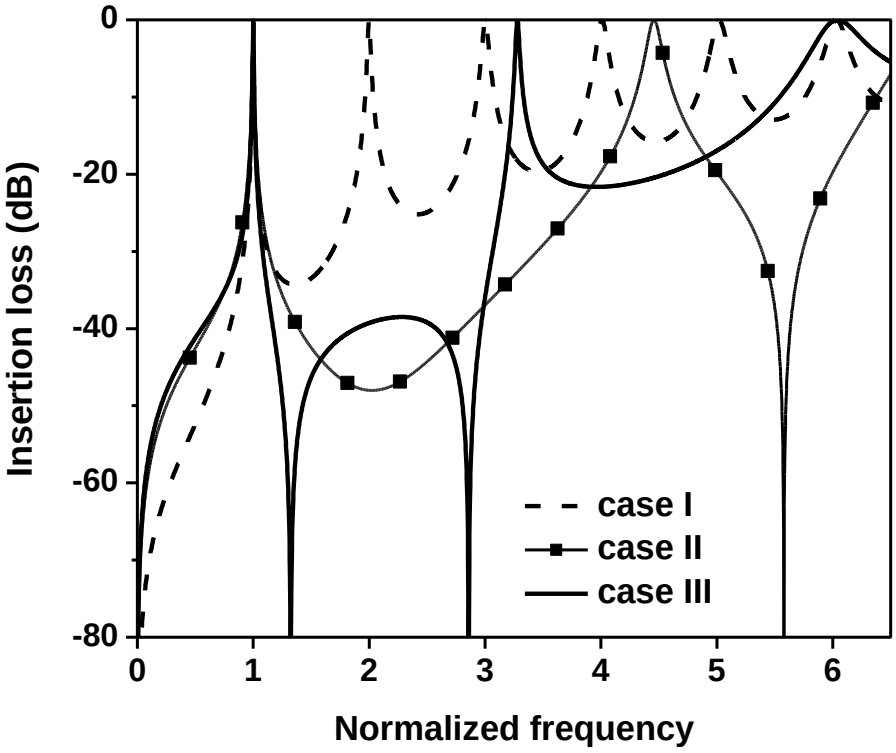

Fig. 19. Simulation results for three cases.

Case II refers to Fig. 18(b) where $\varepsilon_{re} > \varepsilon_{ro}$ while case III is for $\varepsilon_{ro} > \varepsilon_{re}$. Note that similar even-mode impedances (Z_{0e}) and similar odd-mode impedances (Z_{0o}) are assumed for case II and III. Furthermore, $Z_0 = \sqrt{Z_{0e}.Z_{0o}}$, $Z_{0e} > Z_{0o}$ and $\varepsilon_r = \sqrt{\varepsilon_{re}.\varepsilon_{ro}}$. The length of the coupled lines in case II and III is selected to provide the same main resonance as in case I. This results in a length in case II and III to be less than the length in case I.

From the simulation, the second harmonic of the circuit shown in Fig. 18(b) is suppressed for both case II and case III. This suppression is due to the different phase velocities of the even-mode and odd-mode i.e. different ε_{re} and ε_{ro}. Additionally, case III has a sharper and more selective response after the main resonance compared to case I and case II. However, the next repetition of case III apeares lower than in case II.

For well-known microstrip and CPS coupled line, ε_{re} is usually higher than ε_{ro} (case II). To realize case III, i.e. $\varepsilon_{ro} > \varepsilon_{re}$, we propose the use of end-connected broadside coplanar coupled lines (BCCPS) as shown in Fig. 20(a).

The BCCPS consists of four lines: two center lines with width W and two wider lines which serve as ground. These two wider lines are end connected. BCCPS has the ability to be integrated with other CPS lines and also active components in IC design. Furthermore, the broadside coupling can achieve high coupling coefficients. This broadside coupling is implemented without the need for upper and lower grounding cover which is not always available for ICs. In addition, the proposed broadside coupled lines provide freedom to implement more complicated topologies such as the topology proposed in this work. For example implementation of the dashed area in Fig. 18(c) in microstrip requires more layout consideration compared to BCCPS. On the other hand, the proposed topology in Fig. 8(c), requires short resonator lengths compared to the wavelength which makes it suitable especially for IC design.

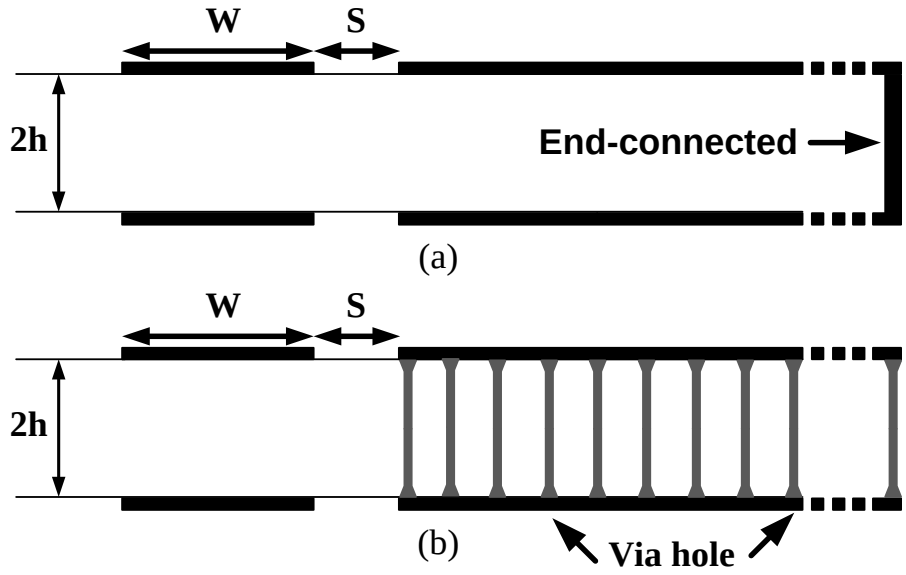

Fig. 20. (a) End-connected BCCPS (b) Entire ground plane connected BCCPS.

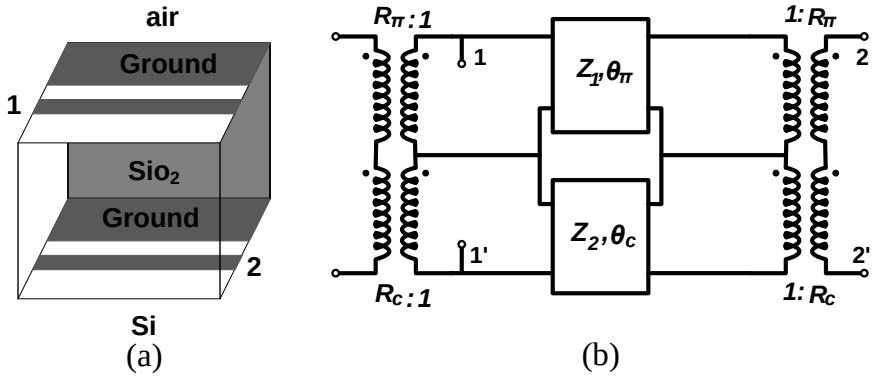

Fig. 21. (a) 3D BCCPS in CMOS (b) Equivalent circuit.

B. Analysis of BCCPS in CMOS

In CMOS, BCCPS acts as an asymmetrical coupled line which leads to two different propagating modes (c-mode and π-mode) [36], [37]. To determine the parameters of the two modes, we applied conformal mapping to the end-connected structure to calculate the self and mutual capacitances and inductances per unit length. In asymmetric BCCPS higher characteristic impedance has lower effective dielectric constant which provides higher selectivity. The derived characteristic impedance and effective dielectric constant for c-mode and π-mode of the end-

connected BCCPS for the model shown in Fig. 21 are summarized in (1)-(10). All C^a refer to the capacitances when the dielectric is replaced with air. c_v is the light speed. K is the complete elliptic integral of the first kind Positive and negative signs in (7) and (8) refer to c-mode and π-mode respectively.

$$C_{12} = \frac{\varepsilon_0 \varepsilon_{r\_sio2}}{2} \left(\frac{K(k_1)}{K(k_1')} - \frac{K(k_1')}{K(k_1)}\right) \tag{1}$$

$$C_{11} = \varepsilon_0 \frac{K(k')}{K(k)} + \varepsilon_0 \varepsilon_{r\_sio2} \frac{K(k_1')}{K(k_1)} + C_{12} \tag{2}$$

$$C_{22} = \varepsilon_0 \varepsilon_{r\_si} \frac{K(k')}{K(k)} + \varepsilon_0 \varepsilon_{r\_sio2} \frac{K(k_1')}{K(k_1)} + C_{12} \tag{3}$$

$$\Delta C^a = C_{11}^a C_{22}^a - (C_{12}^a)^2 \tag{4}$$

$$L_{11} = \frac{C_{22}^a}{c_v^2 \Delta C^a};\ L_{22} = \frac{C_{11}^a}{c_v^2 \Delta C^a};\ L_{12} = \frac{C_{12}^a}{c_v^2 \Delta C^a} \tag{5}$$

$$\lambda = \sqrt{4(L_{12}C_{22} - L_{11}C_{12})(L_{12}C_{11} - L_{22}C_{12}) + (L_{22}C_{22} - L_{11}C_{11})^2} \tag{6}$$

$$R_{c,\pi} = \frac{L_{22}C_{22} - L_{11}C_{11} \pm \lambda}{2(L_{12}C_{22} - L_{11}C_{12})} \tag{7}$$

$$\varepsilon_{c,\pi} = c_v^2 \frac{L_{11}C_{11} + L_{22}C_{22} - 2L_{12}C_{12} \pm \lambda}{2} \tag{8}$$

$$Z_c = \frac{c_v}{\sqrt{\varepsilon_c}} \left(L_{11} - \frac{L_{12}}{R_\pi}\right);\ Z_\pi = \frac{c_v}{\sqrt{\varepsilon_\pi}} \left(L_{11} - \frac{L_{12}}{R_c}\right) \tag{9}$$

$$Z_1 = Z_\pi \left(1 - \frac{R_\pi}{R_c}\right)^{-1};\ Z_2 = Z_c \left(1 - \frac{R_c}{R_\pi}\right)^{-1} \tag{10}$$

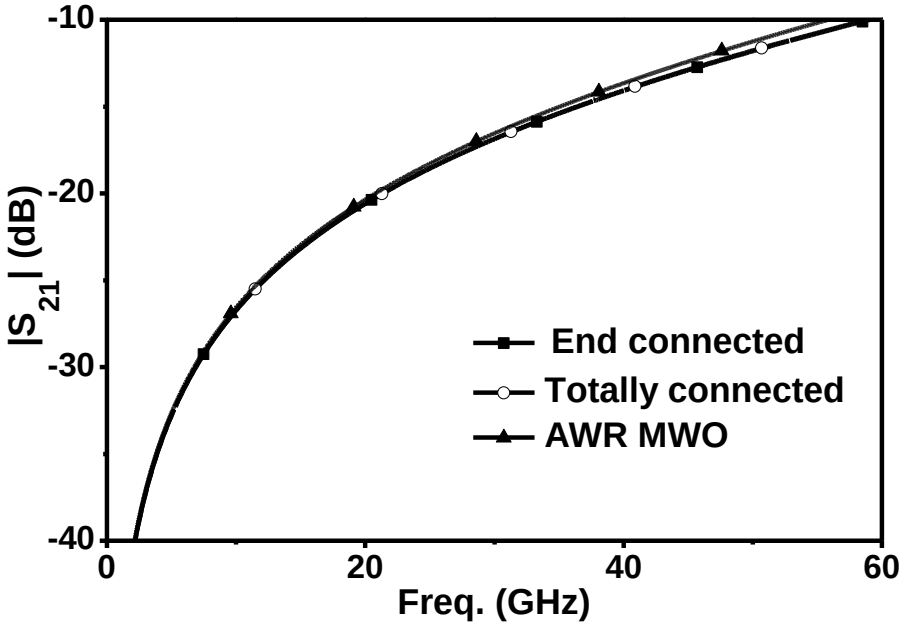

Fig. 22. Schematic modeling versus EM simulations.

ε_{r_Si} and ε_{r_sio2} are silicon and silicon dioxide relative dielectric constant respectively. $k = \sqrt{S/(S+W)}$; $k' = \sqrt{1-k^2}$; $k_1 = \sqrt{x_b(x_a-1)/x_a(x_b-1)}$; $k_1' = \sqrt{1-{k_1}^2}$; $x_a = e^{\frac{\pi S}{h}}$ and $x_b = e^{\frac{\pi(W+S)}{h}}$. To implement the end connection in CMOS, it is possible to use via holes in the ground planes as shown in Fig. 20(b). To verify the effect, a comparison is shown in Fig. 22 between the schematic model in AWR Microwave Office (MWO) based on the derived parameters, and EM simulations in Sonnet when the ground planes are only connected at the end side and when the entire ground planes are connected by via holes for a lossless single BCCPS coupled line section. In the modeling the silicon conductivity is ignored and loss free dielectrics and conductors are assumed. Good agreement is observed between the schematic results and the EM simulation when ground planes are connected using via holes. This comparison proves that, the end connected grounds can be replaced with via holes connecting the two ground strips.

4.3. CMOS K_a band filter using BCCPS section

Fig. 18(c) shows the topology used for the realization of the compact filter. The dashed area requires multilayer implementation. The topology shown in the dashed area provides a resonator with a relatively small length of 0.1λ. Using the coupled line section instead of single resonator in the dashed area in Fig. 18(c) shifts the first undesired harmonic to three times the main frequency. Although the equivalent dielectric constant of the BCCPS is in the order of microstrip, its c-mode dielectric constant is smaller than its π-mode dielectric constant, which is opposite of the c-mode and π-mode dielectric constant for a traditional coupled microstrip line. This phenomena helps to improve the selectivity of the resonator in BCCPS. Furthermore, due to the nature of the BCCPS line, a higher coupling coefficient is achievable compared to microstrip line. Simulations show that for a fixed dielectric constant and equivalent characteristic impedance, a higher Z_1 which is corresponds to the lower dielectric constant reduces the resonance frequency which is a technique to reduce the size of the resonator. Thus, using BCCPS not only makes the topology realizable, it also reduces the size. The value of the capacitors in series should be small enough to make a high Q resonator. In addition, the length of the connecting transmission line *l'* is almost the same as for the coupled lines *l* in Fig. 18(c). Two transmission zeros are added to improve the filter selectivity.

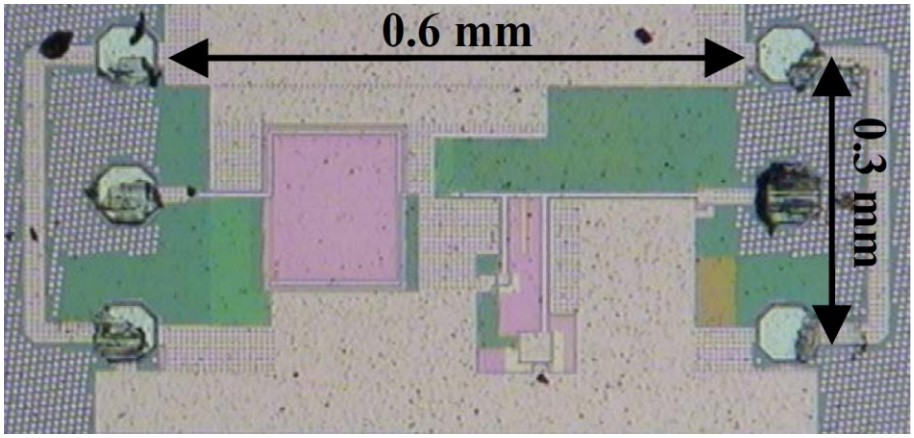

Fig. 23. Photograph of the fabricated filter.

4.4. Filter details

To implement the proposed topology, a BCCPS section with length l=0.1λ at the center frequency of 28.3 GHz and Z_1=112 Ω and Z_2=9 Ω is designed. To connect the end of the upper line to the beginning of the lower line, a high impedance CPS line with the same length (l'= l) is selected. High impedance CPS shifts the resonance frequency to lower frequencies. Optimized values for C and C' are 74 fF and 43 fF respectively. Note that, the dashed area provides a transmission zero at DC. The top metal layer is used for the main conductor. To decrease the conductor loss, M2-M5 are stacked to construct the lower conductor. The added transmission zeros to improve the filter selectivity are implemented by using CPS lines and capacitors. The characteristic impedance of the stub lines is optimized for 75 Ω. The first zero at 17 GHz is realized by the longer line and a capacitor of 1.05 pF to ground. The second zero at 40.5 GHz is realized by the shorter line and a capacitor of 0.15 pF to ground. This design demonstrates the feasibility of integrating BCCPS line with

CPS line. The photograph of the fabricated filter is depicted in Fig. 23. The filter core size is 0.6 x 0.3 mm^2.

4.5. Filter results

Fig. 24 shows the comparison of EM simulations in Sonnet with the measured insertion loss. For low frequencies and the passband, the simulated and measured results match well. The discrepancy at high frequencies might be related to the invalid model for the capacitors at those frequencies. The minimum measured insertion loss is 6.9 dB and the filter shape factor is 0.63. The filter out-of-band rejection below 18 GHz and above 41 GHz is better than 35 dB. The measured insertion loss and return loss of the fabricated filter are also shown in Fig. 25. Table 1 shows a comparison between the presented work with other CMOS filters reviewed here. Since all filters are CMOS filters, λ_o is used as the reference in the size comparison. The 77 GHz filter reported in [39] has a relatively low insertion loss considering the bandwidth. It also has the highest shape factor among other CMOS filters in this table and a reasonable rejection. However, this filter has a comparatively large size which makes implementation in IC at K_a band difficult.

The filter reported in [40], has the smallest size which is due to the semi-lumped implementation of this filter. However, the SF is only in the order of 0.48.

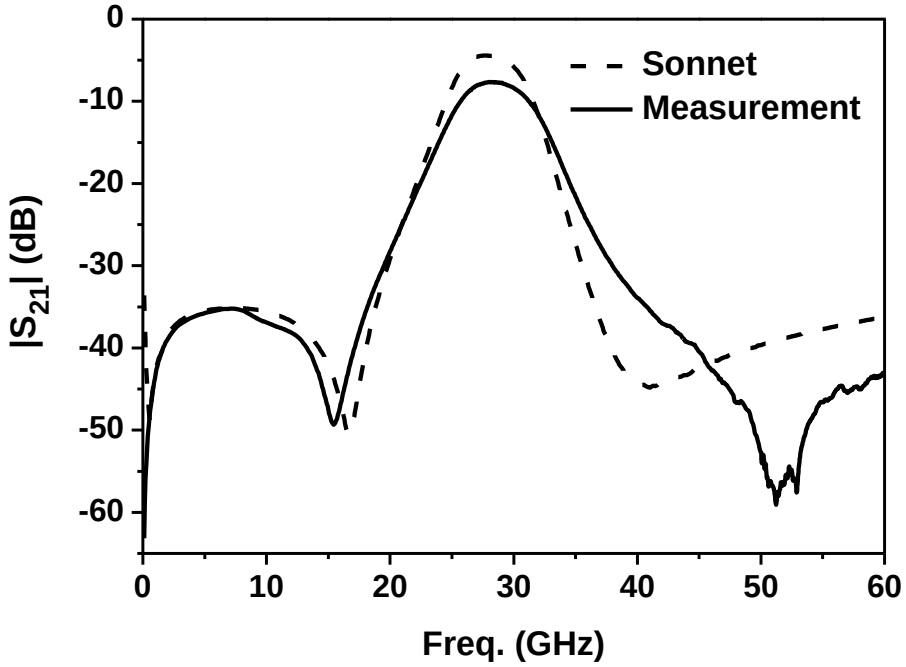

Fig. 24. Simulated and measured insertion loss.

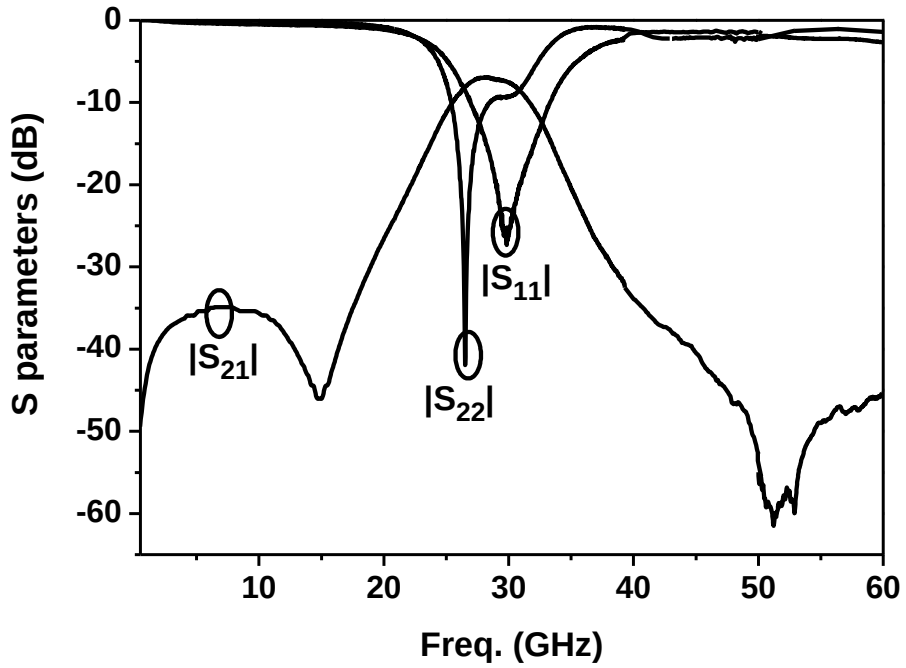

Fig. 25. Measured insertion loss and return loss.

Table 1. Performance comparison of CMOS filters.

	f_o (GHz)	BW (GHz)	3 dB BW (%)	IL (dB)	SF	LR[1] (dB)	Size [2] ($10^{-3}\lambda_o^2$)
[39]	77	70.7-90	24	3.9	0.66	23	5.31
[40]	20	17.9-21.3	17	5.4	0.48	40	0.91
[41]	22	16.8-25.5	41	5.6	0.64	22	2.85
[42]	25	22.5-31.8	31	2.5	0.48	10	1.94
[43]	30	17.5-40	78	2	0.52	8.5	3.97
[44]	35	27.4-45.4	49	4.5	0.59	16	1.65
This work	28.3	25.5-31.6	21	6.9	0.63	35	1.6

[1]LR: Out-of-band rejection below $f_o/2$

[2]Excluded pad chip size where λ_o represents free space wavelength at f_o

Note that, the filter reported in [32], has low insertion loss. Furthermore, the size of this filter is still suitable. However, this filter has a spurious response below the passband which also reduces the filter's shape factor. The filter shape factor and filter rejection of the presented work are improved. Except [30], the work presented here is comparable or smaller than other reported transmission-line filters. However, the filter insertion loss is more than other reported filters considering the bandwidth. The insertion loss can be improved by using more accurate models for the capacitors, by applying loss compensation techniques, and by using an IC process with lower insertion losses.

4.6. Conclusions

A K_a band filter in 0.13 μm CMOS is presented. The filter with improved selectivity consists of BCCPS, CPS sections and MIM capacitors. BCCPS facilitates the realization of a compact resonator with a high coupling coefficient. Furthermore, this resonator introduces a transmission zero at DC. The filter selectivity is furthered improved by adding a zero below and a zero above the passband using stubs and capacitors. The realized filter has small size compared to the wavelength which makes it suitable even for lower frequency IC design. The insertion loss can be reduced by using a lower loss process, improved modeling of components and application of loss compensation techniques.

5. A K_A-BAND LUMPED ELEMENT DUAL-BEHAVIOR RESONATOR (DBR) FILTER IN STANDARD 0.13-µM CMOS TECHNOLOGY

5.1. Introduction

RF filters are essential blocks in modern wireless communication systems. To achieve the goal of System-On-Chip (SOC) design for further reduction of size and cost and to increase functionality, on chip integration of CMOS filters has received considerable interest. Highly selective filters with simple structures are preferred [38]. DBR filters are good candidates because of their simplicity and independently controlled sideband rejections [39]. However, so far, no work has been reported investigating DBR filters in CMOS using lumped components. Here, such a filter is presented.

Typical DBR filters are based on transmission lines and consist of DBRs and quarter wavelength inverters. The DBRs are parallel combinations of different open-circuited stubs or short-circuited stubs [39], [40]. Each stub creates a transmission zero at the fundamental resonant frequency and a passband is formed between the upper and lower rejection zeros. Thus DBR filters allow separate control of the upper and lower stopbands. This is a useful characteristic for duplexer design and for the design of filters with a good shape factor [41]. DBR filters implemented in CMOS technology are reported based on Stepped-Impedance Resonator (SIR) [42] or open stubs [43]. However, these distributed-type chip filters are more suitable for millimeter-wave applications, since they require a large

area when designed at lower microwave frequencies. Semi-lumped DBR filters are also reported for miniaturized filters by loading transmission lines with capacitors [44], [45].

This work proposes a lumped element DBR filter. The filter prototype is implemented in standard 0.13-μm CMOS technology by utilizing CMOS spiral inductors and MIM capacitors. The proposed filter topology can also be used at lower microwave frequencies without increasing the size significantly.

5.2. Lumped Element DBR Filter Design

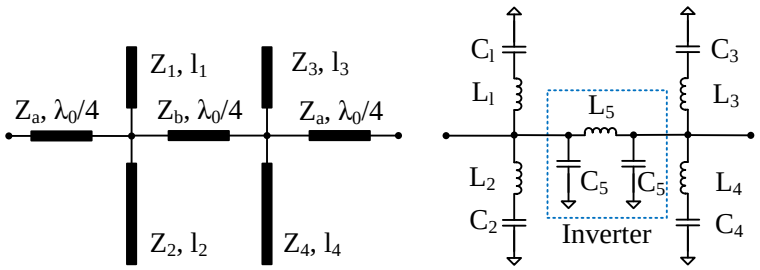

Fig. 26. (a) Traditional second order DBR filter circuit based on open-circuited stubs [3]. (b) Proposed second order lumped element DBR filter with simplified inverters.

Fig. 26(a) shows the circuit of the traditional second order DBR filter with ideal transmission lines based on open-circuited stubs [40]. The first DBR is formed by two open-circuited stubs with characteristic impedance of Z_1 and length l_1 and Z_2 and l_2 respectively. The second DBR is formed by two open-circuited stubs with characteristic impedance Z_3 and length l_3 and Z_4 and l_4 respectively. The DBRs are cascaded by quarter wavelength inverters with characteristic impedance Z_a and Z_b.

To realize the DBR filter using lumped elements, each open-circuited stub is replaced with a shunt branch consisting of a series LC resonator. And the quarter wavelength inverters are realized by an inductor with two shunt capacitors [42]. Fig. 26(b) shows the proposed second order lumped element DBR filter. Note that the inverters in the input and output ports are removed as they are optional and are used for better matching. The lumped element resonators are composed of L_i and C_i (i=1, 2, 3, 4). The center inverter consists of a series inductor L_5 and two shunt capacitors C_5. It is straightforward to determine the transmission zeros of the DBR filter:

$$f_{zero} = \frac{1}{2\pi\sqrt{L_i C_i}} \tag{1}$$

One type of lumped element inverters consists of a series inductor with inductance L and two shunt inductors with inductance $-L$. Here, for the lumped element inverters, shunt capacitors C_5 are used to realize shunt inductors with positive phase shifts. At the center frequency f_c, L_5 and C_5 should satisfy:

$$L_5 C_5 = (2\pi f_c)^2 \tag{2}$$

The lumped elements are realized by on chip spiral inductors and MIM capacitors. The CMOS process used is a standard 0.13-μm process with eight metal layers for the passive components and interconnection. The thickness of the top metal M8 is 3 μm, and the metal of M2 to M7 is 0.42

μm, and M1 is 0.31 μm. To obtain components with the highest Q, symmetrical spiral inductors with only one turn using M8 are and MIM capacitors using M7 and M8 are chosen. Since for the CMOS technology used, the measurement frequency for the inductors and capacitors is only up to 20.05 GHz, the inductors and capacitors are preferred to be as small as possible for accurate design and to avoid a low self-resonant frequency (SRF), and small-value inductors are particularly desired.

The interconnection lines between the lumped elements are 50 Ω microstrip lines in M8. To model the interconnection lines, the CMOS substrate with eight layers is simplified to one layer and is modeled with dielectric constant of 4.0 and thickness of 5.64 μm. The metal at the first layer provides the ground. S parameters of the CMOS passive components are provided by Cadence.

TABLE I: COMPONENTS VALUES OF THE FILTER

Components	$L_{1, 2, 3, 4, 5}$	C_1, C_3	C_2, C_4	C_5
Values	160.3 pH*	289.97 fF	67.95 fF	49.44 fF

* Inductance at the center frequency 27.5 GHz. Inductor's physical parameters: inner core diameter 72.5 μm, conductor width 9 μm, one turn)

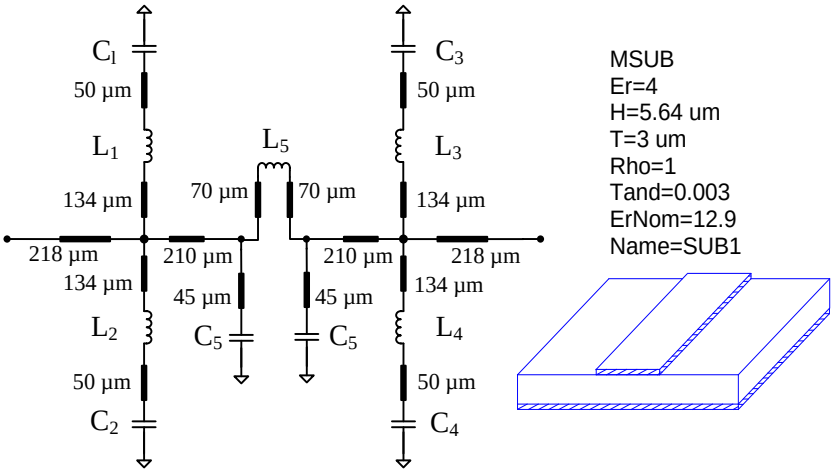

Fig. 27. Schematic simulation in AWR Design Environment.

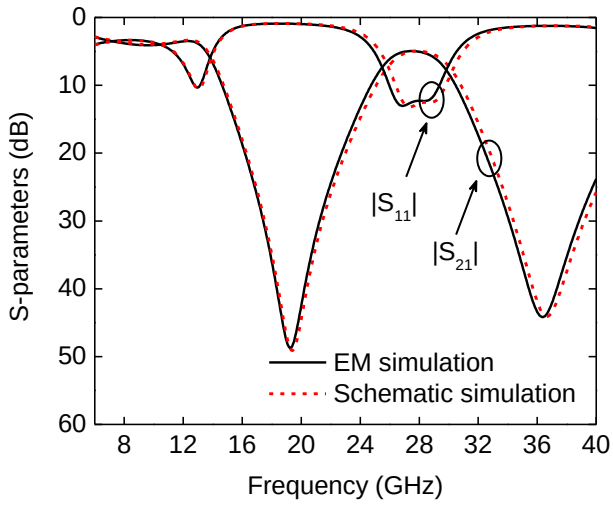

Fig. 28. Responses of schematic simulations and EM simulations.

A prototype filter is designed at the center frequency of 27.5 GHz, with two transmission zeros at 19.3 GHz and 36.3 GHz. Note that this second order DBR filter can realize up to four transmission zeros to achieve wider rejection bands. Here, both DBRs are designed to have the same two transmission zeros to realize a high rejection and high passband selectivity. The values for the components are listed in Table. I. The same spiral inductors are chosen for all inductors to reduce design complexity.

The capacitors are adjusted to obtain required transmission zeros. The schematic simulations are performed in AWR Design Environment. Fig. 27 shows the schematic and substrate settings. Full wave EM simulations for the interconnection lines are performed in Sonnet 13.56. Fig. 28 shows the schematic simulation and the EM simulation results. Both the passband responses and stopband transmission zeros agree well, except that the EM responses are slightly shifted to lower frequencies.

5.3. Experimental Results

Fig. 29 shows the photo of the fabricated filter. The dense metal fillings can be seen beside the filter components. The input and output ports use GSG pads, and the ground pads are connected to M1 ground through via holes from M1 to M8. All MIM capacitors are grounded by connecting M1 to M7 ground through via holes. The total area of the filter is 0.63 mm^2 including the input and output pads.

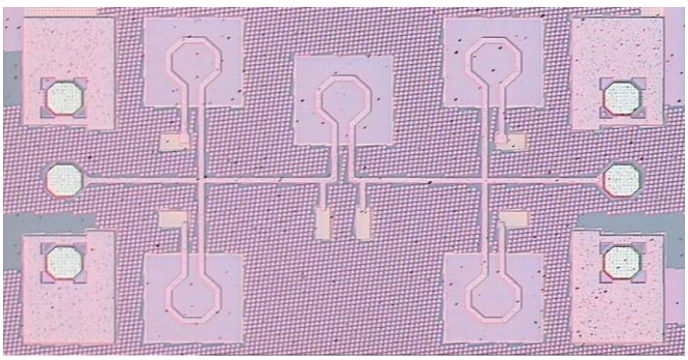

Fig. 29. Photo of the filter.

Fig. 30 and 32 show the EM simulated and measured insertion loss and return loss. The measured insertion loss generally agrees with the

simulated results. The minimum insertion loss is degraded from 5 dB to 7.2 dB. This is likely due to the dense metal filling or inaccurate modeling of the lossy silicon substrate. The measured input return loss is better than 14 dB and output return loss is better than 16.5 dB in the passband. The difference between the measured input return loss and output return loss may be caused by the asymmetrical dense metal filling.

The measured filter achieves a 3-dB bandwidth of 15% and realizes two transmission zeros at 20.2 GHz and 37 GHz. Compared to the reported CMOS DBR filters based on SIRs and open stubs, which obtained notch rejections of 20 dB to 30 dB [42], [43], this filter achieves higher rejections of 48 dB by using lumped elements resonators. This demonstrates that lumped element resonators are useful to create transmission zeros in CMOS chip filter design.

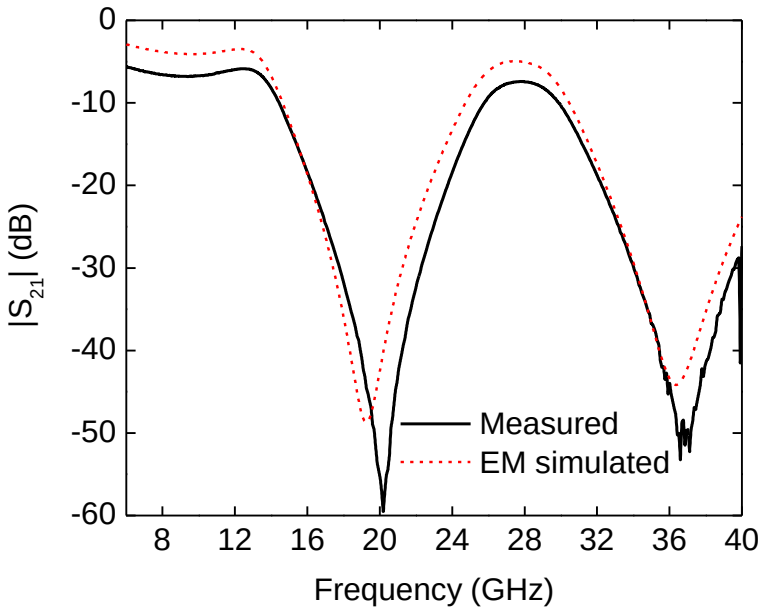

Fig. 30. Simulated and measured insertion loss.

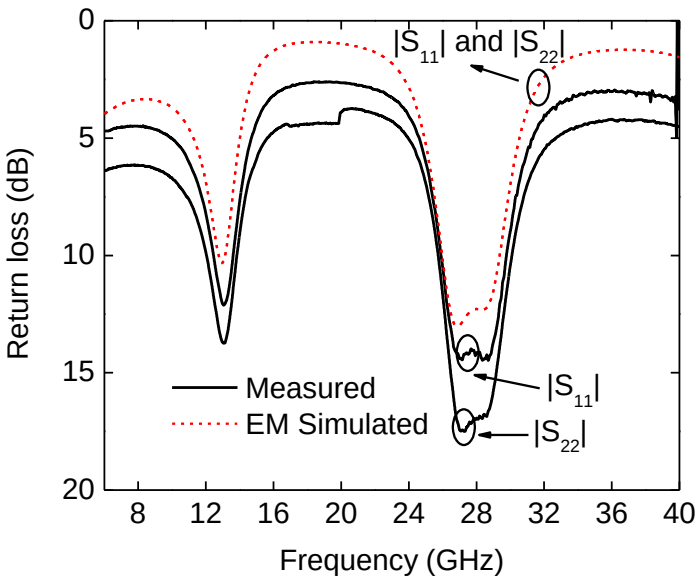

Fig. 31. Simulated and measured return loss.

5.4. Conclusions

A CMOS K_a-band lumped element DBR filter is presented utilizing CMOS spiral inductors and MIM capacitors. The proposed lumped element DBR filter is easy to be implemented which reduces simulation time and design complexity. Moreover, this topology can be used in lower microwave frequency design without increasing the filter size and with improved insertion loss.

The measured filter realizes high notch rejections. This demonstrates that CMOS passive elements are useful components when designing a filter with transmission zeros for a sharper cut-off response.

6. CONCLUSIONS AND FUTURE WORK

In this project, filters for L-band and Ka-band are designed and fabricated in 0.13 μm CMOS technology.

For the L-band filter design, passive and active realizations are presented. For the Ka-band filter design, microstrip topology and lumped topology are presented. It can be concluded that each of them have shown their own strengths and they have generated decent filter performances.

With the growth and thriving of advanced communication techniques like Software-Defined-Radio and LTE, smart filters remain as a research topic. Future work could include:

1. Reconfigurable filters.
2. Loss reduction techniques for passive filters.
3. Active filters with improved large signal behavior.
4. Combination of silicon with SAW resonators.
5. Active filters at K_a band.

References

[1] A. Taslimi, K. Mouthaan, "L-band wideband filter in 0.13 µm CMOS with high common-mode rejection" Microwave Symposium Digest (MTT), 2012 IEEE MTT-S International, pp. 1-3.

[2] F. Hu, K. Mouthaan, "Lossless CMOS active reciprocal two-port inductor and application in a series LC filter" Euro. Microw. Conf. 2012, pp. 364-367.

[3] A. Taslimi, K. Mouthaan, "Compact Ka band filter in 0.13 µm CMOS using broadside coupled coplanar stripline", accepted by Euro. Microw. Conf. 2013.

[4] X.–M. Lu, K. Mouthaan, "A K_a-Band Lumped Element Dual-Behavior Resonator (DBR) Filter in Standard 0.13-µm CMOS Technology", accepted by 2013 APMC.

[5] X.-H. Wang, Q. Xue and W.-W. Choi, "A novel ultra-wideband differential filter based on double-sided parallel-strip line," *IEEE Microw. Wireless Compon. Lett.*, vol. 20, no. 8, pp. 471–473, Aug. 2010.

[6] J. K. Nakaska, J. W`. Haslett, "2 GHz Automatically Tuned Q-Enhanced CMOS Bandpass Filter," in *IEEE MTT-S Int. Microw. Symp. Dig*., Jun. 2007, pp. 1599-1602.

[7] A. M. Abbosh, "Ultrawideband Balanced Bandpass Filter," *IEEE Microw.Wireless Compon. Lett.*, vol. 21, no. 9, pp. 480–482, Sep. 2011.

[8] T. B. Lim and L. Zhu, "Highly Selective Differential-Mode Wideband Bandpass Filter for UWB Application," *IEEE Microw. Wireless Compon. Lett.,* vol. 21, no. 3, pp. 133-135, Mar. 2011.

[9] C.-H. Wu, C.-H. Wang, and C. H. Chen, "Balanced coupled-resonator bandpass filters using multisection resonators for common-mode suppression and stopband extension," *IEEE Trans. Microw. Theory Tech.*, vol. 55, no. 8, pp. 1756–1763, Aug. 2007.

[10] B. Razavi, Design of Integrated Circuits for Optical Communications, New York, McGraw Hill, 2003.

[11] W. R. Eisenstadt, B. Stengel, B. M. Thompson, *Microwave Differential Circuit Design Using Mixed-Mode S S-parameters.* Norwood, MA: Artech House, 2006.

[12] M.–L. Lee, H.-S. Wu, C.-K.-C. Tzuang, "1.58-GHz third-order CMOS active bandpass filter with improved passband flatness," *IEEE Trans. Microw. Theory Tech.*, vol. 59, no. 9, pp. 2275-2284, 2011.

[13] B.-A. Georgescu, I.-G. Finvers, F. Ghannouchi, "2 GHz Q-enhanced active filter with low passband distortion and high dynamic range," *IEEE J. Solid-State Circuits*, vol. 41, no. 9, pp. 2029-2039, 2006.

[14] T. Soorapanth, S.-S. Wong, "A 0-db IL 2140 ± 30 MHz bandpass filter utilizing Q-enhanced spiral inductors in standard CMOS," *IEEE J. Solid-State Circuits*, vol. 37, no. 5, pp. 579-586, 2002.

[15] G. Leuzzi, V. Stornelli, S. Del Re, "A tunable active inductor with high dynamic range for band-pass filter application," *IEEE Trans. Circuits Syst. II, Exp. Briefs*, vol. 58, no. 10, pp. 647-651, 2011.

[16] Z.-Q. Gao, J.-G. Ma, M.-Y. Yu, Y.-Z. Ye, "A fully integrated CMOS active bandpass filter for multiband RF front-ends," *IEEE Trans. Circuits Syst. II, Exp. Briefs*, vol. 55, no. 8, pp. 718-722, 2008.

[17] Y. Wu, X.-H. Ding, M. Ismail, H. Olsson, "RF bandpass filter design based on CMOS active inductors," *IEEE Trans. Circuits Syst. II, Analog and Digital Signal Processing*, vol. 50, no. 12, pp. 942-949, 2003.

[18] F. Hu, K. Mouthaan, "Lossless CMOS active reciprocal two-port inductor and application in a series LC filter," *Eur. Microw. Conf.*, 2012, pp. 364-367.

[19] Y. Chen, P.-I. Mak, L. Zhang, H. Qian, Y. Wang, "A fifth-order 20-MHz transistorized-LC-ladder LPF with 58.2-dB SFDR, 68-μw/pole/MHz efficiency, and 0.13-mm^2 die size in 90-nm CMOS," *IEEE Trans. Circuits Syst. II, Exp. Briefs*, vol. 60, no. 1, pp. 11-15, 2013.

[20] C.-L. Ler, A.-K.-B. A'ain, A.-V. Kordesch. "CMOS active Inductor linearity improvement using feed-forward current source technique" *IEEE Trans. Microw. Theory. Tech.*, vol. 57, no. 8, pp. 1915-1924. 2009.

[21] H. Hayashi, M. Muraguchi, Y. Umeda, T. Enoki, "A high-Q broad-band active inductor and its application to a low-loss analog phase shifter" *IEEE Trans. Microw. Theory Tech.*, vol. 44, no. 12, pp. 2369-2374, 1996.

[22] C.-L. Yang, S.-Y. Shu, Y.-C. Chiang, "Design of a K-band chip filter with three tunable transmission zeros using a standard 0.13-μm CMOS technology," *IEEE Trans. Circuits Syst. II, Exp. Briefs*, vol. 57, no. 7, pp. 522-526, 2010.

[23] A. Thanachayanont, A. Payne, "CMOS floating active inductor and its applications to bandpass filter and oscillator designs" *IEEE Proceedings-Circuits, Devices and Systems*, vol. 147, no. 1, pp. 42-48, 2000.

[24] S Hara., T Tokumitsu, M Aikawa, "Lossless broad-band monolithic microwave active Inductors" *IEEE Trans. Microw. Theory Tech.*, vol. 37, no. 12, pp. 1979-1984, 1989.

[25] G.-F. Zhang, M.-L. Villegas, C.-S Ripoll, "New broadband tunable monolithic microwave floating active inductor" *IET Electron. Lett.*, vol. 28, no. 1, pp. 78-81, 1992.

[26] Q.-T. Lai, J.-F. Mao, "A new floating active inductors using resistive feedback technique" *Microw. Symposium Digest (MTT)*, pp. 1748-1751, 2010.

[27] El Khoury, S. Georges "New approach to the design of active floating inductors in MMIC technology" *IEEE Trans. Microw. Theory Tech.*, vol. 44, no. 4, pp. 505-512, 1996..

[28] A. Thanachayanont, A. Payne, "VHF CMOS integrated active inductor," *IET Electron. Lett.*, vol. 32, no. 11, pp. 999-1000, 1996.

[29] H.-C. Lu, C.-S. Yeh and S.-A. Wei, "Miniaturised 60 GHz rectangular ring bandpass filter in 90 nm CMOS technology," *Electron. Lett*, vol. 47, no. 7, pp. 448 - 450, Mar. 2011.

[30] Y.-M. Chang and S.-F. Chen, "A ultra-compact 77-GHz CMOS bandpass filter using grounded pedestal stepped-impedance stubs," in *2011 European Microwave Conference (EuMC)*, Manchester, 2011, pp. 194-197.

[31] V. Sekar and K. Entesari, "A K-Band Integrated Bandpass Filter in 90-nm CMOS Technology," in *2011 IEEE Radio and Wireless Symposium (RWS)*, 2011, pp. 122-125.

[32] S. Lin, H. Cui, L. Wu, W. Wang and X. Sun, "Design of broadside-coupled parallel line millimetre wave filters by standard 0.18-μm complimentary metal oxide semiconductor technology ," *IET Microw. Antennas Propag.*, vol. 6, no. 1, pp. 72 - 78 , Jan. 2010.

[33] C.-L. Yang, S. -Y. Shu and Y.- C. Chiang, "Design of a K-Band chip filter with three tunable transmission zeros using a standard 0.13-μm CMOS technology," *IEEE Trans. Circuits Syst. II, Exp. Briefs*, vol. 57, no. 7, pp. 522-526, Jul. 2010.

[34] C. H. Doan, S. Emami, A. M. Niknejad, and R. W. Brodersen C. H. Doan, "Millimeter-wave CMOS design," *IEEE J. Solid-State Circuits*, vol. 40, no. 1, pp. 144-155, Jan. 2005.

[35] L.-K. Yeh, C.-Y. Chen and H.-R. Chuang, "A Millimeter-Wave CPW CMOS On-Chip Bandpass Filter Using Conductor-Backed Resonators," *IEEE Trans. Electron Devices*, vol. 31, no. 5, pp. 399 - 401 , My. 2010.

[36] P. A. Rizzi, Microwave engineering, passive circuits. Prentice-Hall, 1988.

[37] C.-M. Tsai and K. C. Guptz, "A generalized model for coupled lines and its applications to two-layer planar circuits," *IEEE Trans. Microw. Theory Tech.*, vol. 40, no. 12, pp. 2190-2199, Dec. 1992.

[38] S. S. Bedair and I. Wolff, "Fast and accurate analytic formulas for calculating the parameters of a general broadside-coupled coplanar waveguide for (M)MIC applications," *IEEE Trans. Microw. Theory Tech.*, vol. 37, no. 5, pp. 843 - 850, May. 1989.

[39] C.-L Yang, S.-Y Shu, Y.-C Chiang, "Analysis and Design of a Chip Filter with Low Insertion Loss and Two Adjustable Transmission Zeros Using 0.18-μm CMOS Technology," *IEEE Trans. Microwave Theory Tech.*, vol. 58, No. 1, pp. 176–184, Jan. 2010.

[40] C. Quendo, E. Rius, and C. Person, "Narrow Bandpass Filters Using Dual Behavior Resonators," *IEEE Trans. Microwave Theory Tech.*, vol. 51, No. 3, pp. 734–743, Mar. 2003.

[41] C. Quendo, E. Rius, and C. Person, "Narrow Bandpass Filters Using Dual Behavior Resonators Based on Stepped-impedance Stubs and Different-length Stubs," *IEEE Trans. Microwave Theory Tech.*, vol. 52, No. 3, pp. 734–743, Mar. 2004.

[42] A. Manchec, E. Rius, et. al, "Ku-Band Microstrip Diplexer Based on Dual Behavior Resonator Filter," 2005 *IEEE MTT-S Int. Microwave Symp*, pp. 525-528, 2005.

[43] L.-K Yeh, C. -Y Hsu, C. -Y Chen and H. -R Chuang, "A 24-/60-GHz CMOS On-Chip Dual-Band Bandpass Filter Using Trisection Dual-Behavior Resonators," *IEEE Electron Device Letters*, vol. 29, No. 12, pp. 1373-1375, Dec. 2008.

[44] A.-L Franc, E. Pistono, N. Corrao, Ph. Ferrari, "Compact High Rejection Notch and DBR Designed with Slow-wave Transmission Lines," 2010 *Asia-Pacific Microw. Conf. Proc. (APMC)*, pp. 1146-1149, 2010.

[45] H. Issa, J. -M. Duchamp, S. Abou-Chahine, and Ph. Ferrari, "Compact Semi-lumped Two-pole DBR Filter with Spurious Suppression," 2011 *Asia-Pacific Microw. Conf. Proc. (APMC)*, pp. 425-428, 2011.

[46] H. Issa, J. -M Duchamp, and Ph. Ferrari, "Miniaturized DBR Filter: Formulation and Performances Improvement," 2008 *IEEE MTT-S Int. Microwave Symp*. pp. 671-674, 2008.

[47] J. S. Hong, M. J. Lancaster, "Microstrip Filters for RF/Microwave Applications," 2001 John Wiley & Sons, Inc., pp. 62.